Fermi National Accelerator Laboratory

FERMILAB-Pub-76/79-EXP
7200.311

(Submitted to Phys. Rev. D)

NEUTRAL PARTICLE PRODUCTION IN 100 GeV/c $\bar{p}p$ INTERACTIONS

R. Raja, C. Moore, L. Voyvodic, and R. J. Walker
Fermi National Accelerator Laboratory, Batavia, Illinois 60510, U. S. A.

and

R. E. Ansorge, C. P. Bust, J. R. Carter, W. W. Neale,
J. G. Rushbrooke, and D. R. Ward
Cavendish Laboratory, Cambridge, England

and

B. Y. Oh, M. Pratap, G. Sionakides, G. A. Smith,
and J. Whitmore
Department of Physics
Michigan State University, East Lansing, Michigan 48824, U. S. A.

September 1976

Operated by Universities Research Association Inc. under contract with the Energy Research and Development Administration

I. INTRODUCTION

We present results on the inclusive production of γ, K^o_s, Λ^o and $\bar{\Lambda}^o$ in 100 GeV/c $\bar{p}p$ interactions. The data described in this paper were obtained from a 98,000 picture exposure of the 30" bubble chamber at Fermilab incorporating the downstream wide gap spark chamber system. Charged multiplicity distributions of $\bar{p}p$ events and their differences with respect to corresponding pp data have already been published[1,2]. In this report we extend these comparisons between $\bar{p}p$ and pp events to neutral particle production and attempt where possible to ascertain the nature of this difference. A preliminary description of the data being presented in this paper has been published elsewnere[3].

From a Regge analysis of the imaginary part of the forward elastic amplitude, it is possible to conclude[4] that

$$\sigma_{\bar{p}p}^{tot} - \sigma_{pp}^{tot} \propto s^{\alpha_\omega(o)-1} \qquad (1)$$

where $\alpha_\omega(o) \approx 0.4$ is the intercept of the ω trajectory. It can also be argued that the difference between the $\bar{p}p$ and pp total cross sections is mainly due to the annihilation

channels present in $\bar{p}p$. On the basis of a generalized multiRegge model developed by Chew, Goldberger and Low[5], it is possible to show[6] that annihilation channels produced by baryon exchange can sum up via unitarity to generate the difference (1). Recently however, Eylon and Harari[7] have argued on the basis of a dual model that the annihilation channels sum up via unitarity to contribute to the Pomeron term in $\sigma_{tot}(\bar{p}p)$ and that the non-annihilation channels contribute to the ω and ρ exchanges in the elastic amplitude. This then implies that the difference in cross sections (1), which falls with s to the power $\alpha_\omega(o)-1$, is due in part to non-annihilation processes. Nonetheless one can still hope to gain some insight into annihilation processes by studying differences, and in fact previous data from this experiment showed[2] that such a non-annihilation contribution might be small.

Experimental details are described in sections II and III, and in section IV we consider topological cross sections for neutral production, and investigate their scaling properties with regard to lower energy data. We also consider the implications of the multiperipheral model of Goldberg[8] for π^0 production in annihilations. Section V describes longitudinal momentum distributions, with particular regard to scaling, and section VI examines transverse momentum distributions. We subsequently discuss effective masses,

missing masses, polarization effects and multiple production of neutrals.

II. EXPERIMENTAL DETAILS

a) The beam. The beam of 100 GeV/c antiprotons was obtained from the decay of $\bar{\Lambda}^0$ particles produced by the interactions of 300 GeV/c protons in a copper target. The charged secondaries from the target were swept away and the $\bar{\Lambda}^0$ particles were allowed to decay in a vacuum pipe. The beam line downstream of the primary target was tuned to accept 100 GeV/c negatives. This resulted in a $\bar{p}/\pi^-$ ratio of ~1:4 in the bubble chamber[9]. By triggering the bubble chamber flash whenever two or more $\bar{p}$'s entered the chamber or whenever a $\bar{p}$ interacted, it was possible to obtain a $\bar{p}/\pi^-$ interaction ratio of 1:1.

b) Fiducial volume cuts and Fitting procedure. We have scanned for and measured all events with an associated "vee". For secondary vertices we employed a fiducial volume whose dimensions were determined by the constraint that it be the largest volume visible in all three views. No event whose primary vertex was more than 10 cm downstream from the center of the chamber was accepted. The measured events were processed by the computer programs TVGP and SQUAW for geometric reconstruction and kinematic fitting . Where possible, ambiguities were resolved at the scanning table by

comparing predicted and observed ionizations. The remaining ambiguities were eliminated by examining the fitted transverse momentum ($p_\perp$) distribution of the tracks of the vee relative to the neutral particle direction. The maximum $p_\perp$ for an electron pair is ~20 MeV/c so any ambiguities with $p_\perp$ < 20MeV/c were assigned to the γ hypothesis. The maximum value of $p_\perp$ for a K_s^o decay is 206 MeV/c whereas for a $\Lambda^o(\bar{\Lambda}^o)$,it is 100 MeV/c. By distributing the K_s^o/Λ^o ambiguities in a manner consistent with the requirement that both $p_\perp$ distributions have the desired shape, the remaining K_s^o/Λ^o ambiguities were resolved statistically. Our detection efficiency for $\bar{\Lambda}^o$ decays is poor since most $\bar{\Lambda}^o$'s go forward in the laboratory with large momenta. The same is true for forward going Λ^o's. We correct for the loss of fast Λ^os by reflecting the $\bar{\Lambda}^o$ events that occur in the backward hemisphere in the center of mass[10], a valid procedure due to C invariance. Unless otherwise stated no $\bar{\Lambda}^o$ information will be explicitly presented, since all $\bar{\Lambda}^o$ distributions may be obtained from the Λ^o distributions by inversion in the center of mass.

III. SCANNING EFFICIENCIES AND WEIGHTS

To each event in the fiducial volume the following weight was attached:

$$WT = \frac{1}{e^{-Lmin/L_o} - e^{-Lpot/L_o}}$$

where Lpot= the potential length of the vee (i.e.,the path length from the primary vertex to the edge of the fiducial volume).

Lmin= the minimum length permitted between the primary and the secondary vertices (= 2 cm. for K_s^o and 3 cm. for $\Lambda^o/\bar{\Lambda}^o$ and γ.) The scanning losses for vees closer to the vertex than Lmin were deemed to be too large to be accurately determined by a second scan.

and

$$\frac{1}{L_o} = \frac{1}{L_D} + \frac{1}{L_I} \quad \text{for } \Lambda^o \text{ and } K_s^o$$

$$= \frac{1}{L_I} \quad \text{for } \gamma$$

where L_D= decay length of the strange particle and L_I= interaction length of the particle.

The correction due to interaction is small for Λ^o and K_s^o events so their interaction lengths were computed by assuming constant total cross sections of 35 mb and 25 mb respectively. These values are the total cross sections for $\Lambda^o p$ scattering[11] and the average of K^+p and K^-p scattering[12]

at the mean laboratory momenta of the Λ^0 and K_S^0 respectively. For gammas with laboratory momenta greater than 40 Mev/c, the cross section for pair production was parametrized as a function of momentum[13]. The pair production cross section falls rapidly for momenta below 40 MeV/c, leading to large weights. It was therefore decided to reject gammas with laboratory momenta less than 40 Mev/c and to correct for this loss by doubling the weights of those forward gammas that yield laboratory momenta less than 40 Mev/c when inverted in the center of mass. This procedure is valid since, due to C invariance, there is inversion symmetry in the center of mass for gammas. The $\cos\theta^*$ distribution with these slow gammas and their corresponding partners removed is symmetric about $\cos\theta^* = 0$ (Fig. 1(a)) indicating that the scanning efficiency for the very forward γ's is similar to that for γ's going backward in the center of mass[14].

The K_S^0 longitudinal momentum distribution in the center of mass (P_L^*) shows losses for positive P_L^* (Fig. 1(b)). It was therefore decided to ignore all forward going K_S^0 and to double the weights of those in the backward hemisphere, invoking C invariance once more. The weight for each event was corrected for the net scanning/measuring efficiency for that channel. For the strange particles, the weights were further corrected for unseen decay modes by dividing by the

branching ratio[15] of the observed decay mode. Table I gives the scanning efficiencies and average weights for each channel.

IV. INCLUSIVE TOTAL AND TOPOLOGICAL CROSS SECTIONS COMPARISON WITH MULTIPERIPHERAL MODEL PREDICTIONS

The weights thus obtained were normalized so that the total number of $\bar{p}p$ interactions with charged multiplicity $\geq$ 4 in the primary vertex fiducial volume corresponded to a cross section of 31.0 ± 0.5 mb[1]. The cross sections are given in ref. 3, which also makes a detailed comparison of $\bar{p}p$ and pp inclusive cross sections.

Dao and Whitmore[16] have proposed an extension of KNO scaling for π^0 production

$$\frac{\langle n\rangle \sigma_n(\pi^0)}{\langle n_{\pi^0}\rangle \sigma_{inel}} = \Phi(n/\langle n\rangle) \qquad (4)$$

and an analogous relationship has been applied by Cohen[17] to K_S^0 and Λ^0 production in pp interactions at high energies. In Fig 2(a-c) we plot $(\langle n\rangle \sigma_n(V^0))/(\langle n_{V^0}\rangle \sigma_{inel}$ against $n/\langle n\rangle$ for π^0, K_S^0 and Λ^0 production in $\bar{p}p$ interactions from 4.6 to 100 GeV/c[18]. For comparison the fits of refs. 16 and 17 to high energy pp interactions are

also shown. We see that the π^0 and K_S^0 topological cross sections scale well over the whole energy range, and lie on top of the pp curves. The Λ^0 data, in contrast, do not scale, the low multiplicity points falling and the high multiplicity points rising with increasing energy. The 100 GeV/c $\bar{p}p \to \Lambda^0$ points agree quite well with the pp data, suggesting that scaling may have been achieved by this energy.

Goldberg[8] has adapted the multiRegge model of Chew, Goldberger and Low to describe the annihilation process $\bar{p}p \to (m)\pi^-(m)\pi^+(k)\pi^0$. Using the "strong ordering approximation" that assumes that the different multiperipheral graphs do not interfere, he finds

$$\sigma_{m,k} = G^4 e^{(2\alpha_B - 2)Y} (g^2 Y)^{2m+k-2} \left(\frac{1}{3}\right)^k \left(\frac{2}{3}\right)^{2m} \times \frac{(2m+k)!}{k!\,2m!\,(2m+k-2)!} \qquad (5)$$

where $\sigma_{m,k}$ is the cross section for $\bar{p}p$ annihilation into $(m)\pi^-, (m)\pi^+$ and $(k)\pi^0$. The notation follows ref. 8. From (5) the topological cross section σ_m for the process $\bar{p}p \to (m)\pi^-(m)\pi^+$ may be computed, yielding

$$\sigma_m = \sum_{k=0}^{\infty} \sigma_{m,k} = G^4 e^{(2\alpha_B - 2 + g^2/3)Y} \left[\frac{4}{9} \frac{(\frac{2}{3} g^2 Y)^{2m-2}}{(2m-2)!} + \frac{4}{9} \frac{(\frac{2}{3} g^2 Y)^{2m-1}}{(2m-1)!} + \frac{1}{9} \frac{(\frac{2}{3} g^2 Y)^{2m}}{(2m)!}\right]$$

and $\sigma_{annih} = \sum_{m=0}^{\infty} \sigma_m \quad \simeq \frac{1}{2} G^4 e^{(2\alpha_B - 2 + g^2)Y}$ (6)

Following Goldberg we now impose the bootstrap condition that

$$2\alpha_B - 2 + g^2 = \alpha_\omega(0) - 1 \simeq -0.6 \qquad (7)$$

assuming that $\sigma_{annih} = \sigma_{\bar{p}p}$ (tot) $- \sigma_{pp}$ (tot). If one now further assumes that σ_m is the difference in topological cross sections between $\bar{p}p$ and pp[19] of multiplicity n=2m, one can fit the differences to equation (6) subject to the constraint (7). Table II contains a summary of the results of such a fit.[20]

We can now predict the difference between $\bar{p}p \to \pi^0$ and $pp \to \pi^0$ inclusive cross sections as a function of the charged multiplicity. However the errors are large so that only the gross features may be trusted. Using equation (5) we derive

$$\sigma_n(\bar{p}p \to \pi^0) - \sigma_n(pp \to \pi^0) = \sum_{k=0}^{\infty} k\sigma_{m,k} \qquad n = 2m$$
$$= G^4 \frac{e^{(2\alpha_B - 2)Y}}{2m!} (g^2 Y)^{2m-2} \left(\frac{2}{3}\right)^{2m} e^x \left[2m\,(2m+1)x + 2(2m+1)x^2 + x^3\right]$$
$$\text{where } x = \frac{g^2 Y}{3} \qquad (8)$$

Using the fitted values of G^4, g^2 and α_B yields a total

predicted excess for $\bar{p}p$ over pp of 16±2 mb in the charged multiplicity range 4-18. The experimental value is 7.1±6.7 mb[3], about one standard deviation lower. The model predicts a mean neutral multiplicity half that of the mean charged multiplicity in the same prong range.

The last column in Table II contains the prediction of the model for the mean number of π^0's produced in annihilation processes as a function of the number of charged pions. The mean number of π^0's is predicted to be almost independent of the charged pion multiplicity at these energies. This is in marked contrast to the experimentally observed correlation between the mean number of π^0's and charged primary multiplicity in pp interactions, or in the overall sample of this experiment[3]. Thus this prediction could prove a useful test of the model, though the errors on ($\bar{p}p$-pp) differences in the present experiment are too large to allow any conclusions to be drawn.

V. LONGITUDINAL DISTRIBUTIONS

Rapidity distributions. Any attempt to make a detailed comparison of differential distributions between $\bar{p}p$ and pp data is difficult due to the limited statistics . However, the $\bar{p}p$ inclusive cross sections are higher than the corresponding pp values, and the trend of low energy data

tends to reinforce this view. The differential distributions reflect this excess in normalization but in most cases we cannot attach any dynamical significance to the observed differences in differential distributions[3] due to the poor statistics.

Figure 3(a) shows the variation of $d\sigma/d|y^*|$ vs. y^* for γ's where y^* is the center of mass rapidity. The pp data are also shown[21]. The difference of 11 mb mostly occurs in the central region. If this difference persists with higher statistics, then one may conclude that the difference between $\bar{p}p \to \pi^0$ and $pp \to \pi^0$ is concentrated mostly in the central region.

Figure 3(b) shows the corresponding plot for K_S^0 again comparing with pp data[21]. Apart from the difference in overall normalization no significant differences are observed between the $\bar{p}p$ and pp data.

Figure 3(c) shows the variation of $d\sigma/dy^*$ vs. y^* for $\bar{p}p \to \Lambda^0/\bar{\Lambda}^0$ in the backward hemisphere. The $\bar{\Lambda}^0$ contribution to the pp data has been estimated by uniformly distributing the $\bar{\Lambda}^0$ total cross section throughout the range $-0.5<y^*<0.5$. The $\bar{p}p \to \Lambda^0/\bar{\Lambda}^0$ curve is higher than

the $pp \to \Lambda^0/\bar{\Lambda}^0$ curve in the central region. There may thus be an excess of $\Lambda^0/\bar{\Lambda}^0$ produced in $\bar{p}p$ interactions in the central region, although any such assertion can only be tentative in view of the current statistical accuracy of this experiment.

Figures 3(a-c) also show the recoiling mean primary charged multiplicity and the mean transverse momentum as a function of the rapidity of the neutral particle. A rise in recoiling multiplicity is observed towards the central region for $\Lambda^0/\bar{\Lambda}^0$ and K^0_S. One cannot however attribute this solely to annihilations since a similar effect is observed in pp interactions[14]. The mean transverse momenta show a rise towards $y^*=0$ in each case.

<u>Invariant cross sections.</u> Figures 4(a-c) show the invariant distributions

$$F_1(x) = \int \frac{2Ed^2\sigma}{\pi\sqrt{s}dxdp_T2} \quad dp_T2 \quad \text{for the three types}$$

of particles. Also shown are 100 GeV/c pp[21-22] data and 14.75 GeV/c $\bar{p}p$[23] data. There is evidence for scaling in $\bar{p}p \to \Lambda^0$ from 14.75 GeV/c to 100 GeV/c as can be seen from Figure 4(c). Scaling has not set in by 14.75 GeV/c for K^0_S as can be seen from Figure 4(b). The 100 GeV/c $\bar{p}p$

data are quite similar to the 100 GeV/c pp data, any differences being obscured by errors. This can probably be taken as evidence that $\bar{p}p$ and pp data scale according to a common function in the limit of infinite energies.

Also plotted in Figure 4 are the mean values of p_T as a function of x. For γ's and Λ^0s we observe a drop in $\langle p_T \rangle$ for small values of x . For K^0_s, $\langle p_T \rangle$ does not show any significant variation with x.

To examine scaling in the central region in greater detail we plot in Fig 4(d-f) $F_1(0)$ against $s^{-1/4}$ for the production of neutrals in $\bar{p}p$ and pp interactions.[18-24] According to Mueller-Regge theory $F_1(0)$ varies as $(a+bs^{-1/4})$ for large s where a and b are constants. In the case for γ and K^0_s we see that $F_1(0)$ in $\bar{p}p$ is systematically higher than in pp interactions, and both are still rising with energy up to 100 GeV/c. For Λ^0 production, in contrast, $F_1(0)$ seems to be constant from ~10 GeV/c upwards, and about equal in $\bar{p}p$ and pp interactions. We note however that in $\bar{p}p$ there is equal production of $\bar{\Lambda}^0$ at x=0, which is largely absent in pp, thus indicating an overall excess of hyperon and anti-hyperon production in the central region in $\bar{p}p$. These scaling properties are in contrast with the topological

scaling discussed in section IV, where γ and K_S^0 showed good agreement with scaling, while the Λ^0 data changed considerably with energy.

Feynman x distributions. Figures 5(a-c) show $d\sigma/dx$ vs x for the three types of particles. Also shown are the mean values of the recoiling primary charged multiplicity as a function of x. A rise in primary multiplicity is once again observed for Λ^0's toward the central region whereas little x dependence is observed for γ's and K_S^0's.

VI. TRANSVERSE DISTRIBUTIONS

Figure 6(a) plots $d\sigma/dp_T^2$ against p_T^2 for γ's. The data indicate that the difference in normalization between $\bar{p}p$ and pp of 11 mb comes preferentially from small values of p_T^2 and that the mean value of p_T^2 is less for $\bar{p}p$ than pp (see table III). This is however in contrast to the well-known result that annihilation processes at lower energy produce secondaries with a larger average transverse momentum than that found in non-annihilation processes.[25]

Figure 6(b) is the corresponding plot for K_S^0. We see no significant differences in shape between $\bar{p}p$ and pp.

Figure 6(c) shows the variation of $d\sigma/dp_T^2$ vs. p_T^2 for Λ^0. Also shown is $\frac{1}{2}d\sigma/dp_T^2$ vs. p_T^2 for pp data[26]. The $\bar{p}p$ data seem to fall off more sharply than the pp data. This is reflected in the mean value of p_T^2 for Λ^0 which is 0.302±0.023 for $\bar{p}p$ compared to 0.336±0.035 for pp.

The mean values of the recoiling primary multiplicity are plotted as a function of p_T^2 in Figures 6(a-c). There is a discernible rise in primary multiplicity for higher values of p_T^2 for γ's and K_s^0 but very little for Λ^0's. The particle that exhibits the largest change in primary multiplicity in the longitudinal variable exhibits the least change in the transverse variable and vice versa. We also show in Fig. 6(d-f) the variation of $\langle p_T \rangle$ with multiplicity. $\langle p_T \rangle$ seems to be independent of multiplicity within errors for γ and Λ^0, while there is some indication of a rise in $\langle p_T \rangle$ with multiplicity for K_s^0.

Table III summarizes the mean values of p_T and p_T^2 for the three types of particle. The mean value of p_T increases with the mass of the produced particle, in a manner similar to pp data.

VII. MOMENTUM TRANSFER SQUARED DISTRIBUTION FOR LAMBDAS

Figure 7 shows $d\sigma/dt'$ vs t' for Λ^0's, where $t'=t-t_{min}$, t being the square of the momentum transfer between the Λ^0 and

the target proton. A break is observed at a $|t'|$ value of 2.8 $(GeV/c)^2$. A maximum likelihood fit to the functional form

$$\frac{d\sigma}{d|t'|} = Ae^{-B|t'|} \qquad (10)$$

for the two segments yields the following values of A and B:

$A = 2.26 \pm 0.56$ mb/$(GeV/c)^2$
$B = 1.28 \pm 0.32$ $(GeV/c)^{-2}$
for $|t'| < 2.8$ $(GeV/c)^2$

$A = 0.159 \pm .033$ mb/$(GeV/c)^2$
$B = 0.24 \pm 0.05$ $(GeV/c)^{-2}$
for $|t'| > 2.8$ $(GeV/c)^2$

VIII. EFFECTIVE MASSES

Figure 8(a) is a plot of $d\sigma/dM$ vs. M where M is the effective mass of the $K_S^0\pi^\pm$ combination. Each $K\pi$ combination is entered once in the plot. All tracks are assumed to be pions at the primary vertex unless the observed ionization favored a proton. We see a pronounced peak near the mass value of the $K^*(890)$. To estimate the background, we computed the effective mass by associating each kaon with the charged particles from the next event that has a kaon. The dotted curve in Fig. 8(a) is our

estimate for this background. We see that the peak at 890 MeV is almost completely reproduced by the background. We thus see no evidence for $K^*(890)$ production. No signal was seen in the $K_S^0\pi^-$ and $K_S^0\pi^+$ combinations separately. At the one standard deviation level we can quote an upper limit $\sigma(\bar{p}p \rightarrow K^*(890)) < 0.45$ mb.

Figure 8(b) is the effective mass distribution for all $\Lambda^0\pi^\pm$ combinations with the background calculated similarly. Some evidence for the production of $\Sigma(1385)$ is present and after correcting for branching ratios we estimate a cross section for $\Sigma(1385)$ production of 0.24 ± 0.20 mb,this occuring almost entirely in the $\Lambda^0\pi^+$ combination.

Figures 9(a-b) give the effective mass distribution of $K_S^0\pi^+\pi^-$ and $\Lambda^0\pi^+\pi^-$ combinations respectively. All charged particles were assumed to be pions unless ionization data favored a proton. No significant peak in either channel is seen.

IX. MISSING MASS DISTRIBUTIONS

Figures 10(a-c) give the distribution of the square of the missing mass recoiling from γ's, K_S^0's and Λ^0's respectively. Superimposed is the mean recoiling multiplicity in each case. It can be seen that the mean

multiplicity rises with the missing mass squared in much the same way as average multiplicities do with s. Figure 11 compares the recoiling multiplicities for the three types of particle as a function of missing mass squared with $\pi^- p$ and $K^- p$ direct channel data. The data seem to lie on a single universal curve. The agreement is probably better than it seems at first glance, since for the low lying K_S^0 and Λ^0 points the statistics are so poor as to make the estimation of errors in the mean values unreliable. The $\pi^- p$ and $K^- p$ data have had the elastic two prongs subtracted whereas for strict comparison they should be included. This should make the agreement between the missing mass data (which can be thought of as being due to the scattering of the exchanged particle and the particle at the other vertex) and the direct channel data even better.

X. POLARIZATION

We observe a Λ^0 polarization[27] of -0.45 ± 0.21. In computing the polarization we have followed the conventions described in Ref. 14. Figure 12 shows the variation of the polarization with Feynman x. There seems to be a possible trend towards negative values of polarization for x near -1 and 0 . This contrasts with the result obtained for 205 GeV/c pp interactions, where an average Λ^0 polarization consistent with zero was observed[14].

XI. MULTIPLE V^0 EVENTS

From events with two or more vees associated we have calculated the cross sections in Table IV for the production of pairs of neutral particles. Here we have used the forward K_s^o and $\bar{\Lambda}^o$ and compensated for the losses by artificially increasing their decay weights in the forward hemisphere till the sum of weights in the forward hemisphere was equal to the sum of weights in the backward hemisphere for K_s^o and Λ^o respectively.

From the cross section for producing two γ's we can estimate the correlation function f_2^{00} , which can be shown to equal

$$f_2^{00} = \frac{\sigma(2\gamma)}{2\sigma_{inel}} - 0.5\langle n(\pi^o)\rangle - \langle n(\pi^o)\rangle^2 = 3.6\pm2.1 \qquad (11)$$

We note that f_2^{00} is larger than f_2^{--} [1] or f_2^{0-} [3] .We can also calculate the mean numbers of π^o produced in events with Λ^o or K_s^o associated.

$$\langle n(\pi^o)\rangle_{K_s^o} = 2.0\pm0.5 \quad \langle n(\pi^o)\rangle_{\Lambda^o} = 2.4\pm0.7.$$

These values are similar to the overall mean number of π^o produced per inelastic collision:2.64±0.16[3]

The two particle inclusive cross sections are given in Table IV.

XII. CONCLUSIONS

We have examined the production of neutral particles in 100 GeV/c $\bar{p}p$ interactions. Our main findings are as follows:

(i) The topological cross sections for π^0 and K_S^0 production, but not for Λ^0, scale with low energy data. The multiperipheral model makes a clear prediction for the numbers of π^0 produced in annihilations.

(ii) The invariant cross section for Λ^0 production scales from 14.75 GeV/c, while γ and K_S^0 do not.

(iii) γ and Λ^0 show slightly lower values of p_T than in pp interactions at this energy.

(iv) We find evidence of $\Sigma(1385)$ production, but no significant $K^*(890)$ signal.

(v) There is evidence of a non-zero Λ^0 polarization.

REFERENCES

[1] R.E.Ansorge et al., Phys. Lett. 59B, 299 (1975).

[2] J.G.Rushbrooke et al., Phys. Lett. 59B, 303 (1975).

[3] D.R.Ward et al. ,Phys. Lett. 62B, 237 (1976).

[4] R.Arnowitt and P.Rotelli,Lett. Nuovo Cimento 4,179 (1970).

[5] G.F.Chew,M.Goldberger and F.Low,Phys.Rev.Lett.22,208 (1968).

[6] P.D.Ting, Phys. Rev. 181, 1942 (1969).

[7] Y.Eylon and H.Harari, Nucl. Phys. B80, 349 (1974).

[8] H.Goldberg, Phys. Rev. D6, 2542 (1972).

[9] W.W.Neale, Fermilab FN-259 (unpublished) 1974.

[10] Reflecting the backward $\bar{\Lambda}^{o}$'s and averaging with the forward Λ^{o}'s leads to a lower cross section of 2.04±0.16 mb for inclusive Λ^{o} production.

[11] S.Gjesdal et al, Phys Lett 40B, 152 (1972).

[12] Compilation of $K^{\pm}p$ interactions CERN-HERA 72-2 (1972)

[13] T.M.Knasel,Desy Reports 70/2 and 70/3 (1970), Unpublished.

[14] K.Jaeger et al., Phys. Rev. D11,2405, (1975).
We note that the authors report a depletion of forward gammas which is attributed to scanning losses.

[15] Particle Data Group, Phys. Lett. 50B, 1 (1974).

[16] F.T.Dao and J.Whitmore Phys. Lett. 46B, 252 (1973).

[17] D.Cohen, Phys. Lett. 47B, 457 (1973).

[18] $\bar{p}p$ data taken from:
4.6 and 9.1 GeV/c P.Gregory: paper submitted to International Symposium on $\bar{N}N$ interactions, Stockholm (1976).

12 GeV/c D.Bertrand et al: Stockholm (1976)

14.75 GeV/c ref 23.

32 GeV/c F.Grard: Stockholm (1976).

[19] C.Bromberg et al., Phys.Rev.Lett.31, 1563 (1973).

[20] Only topological data for greater than or equal to 4 prongs were used in the fit. We have assumed that the difference $\sigma_n(\bar{p}p) - \sigma_n(pp)$ can be attributed to annihilations and this manifestly is not the case for two prongs, the difference being negative[2]. As input to the fit, we have smoothed the values of the differences keeping the normalization constant.

[21] J.W.Chapman et al., Phys. Lett. 47B, 465 (1973).

[22] M.Alston-Garnjost et al., Phys.Rev.Lett.35, 142 (1975).

[23] F.T.Dao et al., Phys. Lett. 51B, 505 (1974).

[24] pp data taken from:

12and24 GeV/c V.Blobel et al. Nucl Phys. B69, 454 (1974)

69 GeV/c H.Blumenfeld et al Phys.Lett. 45B, 525 (1973); ibid 528.

100 GeV/c refs. 21 and 22.

205 GeV/c ref 14.

303 GeV/c A.Sheng et al. Phys. Rev. D11, 1733(1975).

[25] D.Everett et al. Nucl. Phys. B73, 440 (1974).

[26] Strictly the comparison should be $\frac{1}{2}[d\sigma/dp_T^2(\Lambda^o) + d\sigma/dp_T^2(\bar{\Lambda}^o)]$ for pp but since the inclusive $pp \to \bar{\Lambda}^o$ cross section is only 7% of the $pp \to \Lambda^o$ cross section this should not make too much difference to the comparison.

[27] It must be pointed out that the $\bar{p}$'s in this experiment are longitudinally polarized as they are produced by the decay of $\bar{\Lambda}^{o}$'s , though it seems unlikely that this could affect the polarization of Λ^{o}'s produced backward in the CMS.

TABLE I

SCANNING EFFICIENCIES AND WEIGHTS

	γ	K_S^0	Λ^0
Scanning Efficiency	92.5%	92.4%	92.4%
Measuring Efficiency	94.5%	94.5%	94.5%
Kinematics Efficiency	95.4%	97.0%	97.0%
Mean Decay Weight	59.3	2.75	2.28
Standard Deviation	38.0	1.46	0.91
Mean net Weight	71.02	3.23	2.68
Standard Deviation	45.56	1.72	1.08

TABLE II

MULTIPERIPHERAL ANALYSIS

Prong	Experimental values $\sigma_n(\bar{p}p)-\sigma_n(pp)$ mb smoothed	Fitted $\sigma_n(\bar{p}p)-\sigma_n(pp)$ mb	Experimental $\sigma_n(\bar{p}p\to\pi^0)-\sigma_n(pp\to\pi^0)$ mb	Predicted Values $\sigma_n(\bar{p}p\to\pi^0)-\sigma_n(pp\to\pi^0)$ mb	Predicted $\langle\pi^0\rangle$ for annihilations
4	0.30 ± 0.28	0.12 ± 0.05	0.90 ± 1.90	0.63 ± 0.23	5.33 ± 1.30
6	0.65 ± 0.28	0.44 ± 0.14	0.00 ± 4.90	2.24 ± 0.56	5.11 ± 1.25
8	1.13 ± 0.35	0.80 ± 0.15	2.70 ± 3.00	4.01 ± 0.56	4.97 ± 1.25
10	0.61 ± 0.28	0.88 ± 0.10	0.70 ± 1.80	4.25 ± 0.60	4.86 ± 1.20
12	0.34 ± 0.27	0.62 ± 0.12	0.60 ± 1.40	2.97 ± 0.79	4.78 ± 1.20
14	0.30 ± 0.08	0.31 ± 0.10	2.90 ± 1.92	1.46 ± 0.63	4.72 ± 1.20
16	0.15 ± 0.06	0.11 ± 0.08	-0.80 ± 0.45	0.53 ± 0.50	4.67 ± 1.10
18	0.07 ± 0.03	0.03 ± 0.07	0.10 ± 0.64	0.15 ± 0.40	4.63 ± 1.10
Total	3.55 ± 0.66 mb	3.32 ± 0.38 mb	7.10 ± 6.7 mb	16.3 ± 2.0 mb	

Fitted Values $G^4 = 167 \pm 20$ mb.

$g^2 = 2.36 \pm 0.6$

$\alpha_B = -0.48 \pm 0.1$ $\chi^2/\text{D.F.} = 0.96$

TABLE III

MEAN TRANSVERSE MOMENTA

	γ		K_S^0		Λ^0	
	$\bar{p}p$	pp^{21-22}	$\bar{p}p$	pp^{21-22}	$\bar{p}p$	pp^{21-22}
$\langle p_T \rangle$	0.159	0.175	0.470	0.424	0.490	0.541
(GeV/c)	±0.006	±0.020	±0.018	±0.043	±0.020	±0.060
$\langle p_T^2 \rangle$	0.043	0.056	0.295	0.240	0.302	0.336
$(GeV/c)^2$	±0.003	±0.005	±0.022	±0.040	±0.023	±0.035

TABLE IV

CROSS SECTIONS FOR MULTIPLE V^0 PRODUCTION

channel	no.of events	cross section (mb).
$\gamma\gamma$	49	820±140
$K^0_S\gamma$	25	20.8±4.6
$\Lambda^0\gamma$	13	11.2±3.3
$\Lambda^0 K^0_S$	8	0.54±0.21
$K^0_S K^0_S$	11	0.8±0.3
$\Lambda^0\bar{\Lambda}^0$	4	0.7±0.4

FIGURE CAPTIONS

Fig.1: (a) Distribution of CMS angle, $\cos\theta^*$, for γ's after weighting. Events with $p_{lab} < 40$MeV/c and corresponding forward γ's are not included. (b) Longitudinal momentum distribution in CMS for K^o_s. Note the depletion for $p^*_L > 0$.

Fig.2: Scaling of topological cross sections.
(a) $\langle n\rangle\sigma_n(\pi^o)/\langle n_{\pi^o}\rangle\sigma$inel against $n/\langle n\rangle$ for $\bar{p}p \to \pi^o$ at various energies. (b) for K^o_s (c) for Λ^o. The curves are fits to high energy pp data.

Fig.3: Center of mass rapidity distributions for (a) γ's, (b) K^o_s and (c) $\Lambda^o(\bar{\Lambda}^o)$. Also shown are mean multiplicities and mean transverse momenta as a function of rapidity.

Fig.4: The invariant cross section $F_1(x) = \int \frac{2Ed^2\sigma}{\pi\sqrt{s}dxdp_T2} dp_T2$

vs. x for (a) γ, (b) K^o_s and (c) Λ^o
Also shown are mean values of P_T vs x.
(d) $F_1(0)$ for $pp \to \Lambda^o$ and $\bar{p}p \to \Lambda^o$ as a function of $s^{-1/4}$. (e) for K^o_s (f) for γ.

Fig.5: Feynman x distribution for (a) γ, (b) K^o_s and (c) Λ^o also shown are mean values of recoiling primary multiplicity vs. x

Fig.6: P^2_T distribution for (a) γ (b) K^o_s (c) Λ^o
Also shown are mean values of recoiling primary multiplicity as a function of p^2_T. (d) $\langle p_T\rangle$ vs. n

for γ's (e) for K_s^o (f) for Λ^o .

Fig.7: $t' = t - t_{min}$ distribution for Λ^o.

Fig.8: (a) $K_s^o \pi^{\pm}$ effective mass distribution.

The background has been calculated by associating K_s^o with the charged particles from the next event with a K_s^o .

(b) $\Lambda^o \pi^{\pm}$ effective mass distribution. The background has been calculated as in (a).

Fig.9: (a) $K_s^o \pi^+ \pi^-$ effective mass distribution.

(b) $\Lambda^o \pi^+ \pi^-$ effective mass distribution.

Fig.10: Missing mass squared distribution for (a) γ

(b) K_s^o and (c) Λ^o Also shown is the recoiling charged multiplicity as a function of missing mass squared.

Fig.11: Comparison of the variation of recoiling multiplicities vs. missing mass squared with direct channel $\pi^- p$ and $K^- p$ data.

Fig.12: Polarization of Λ^o vs. x.

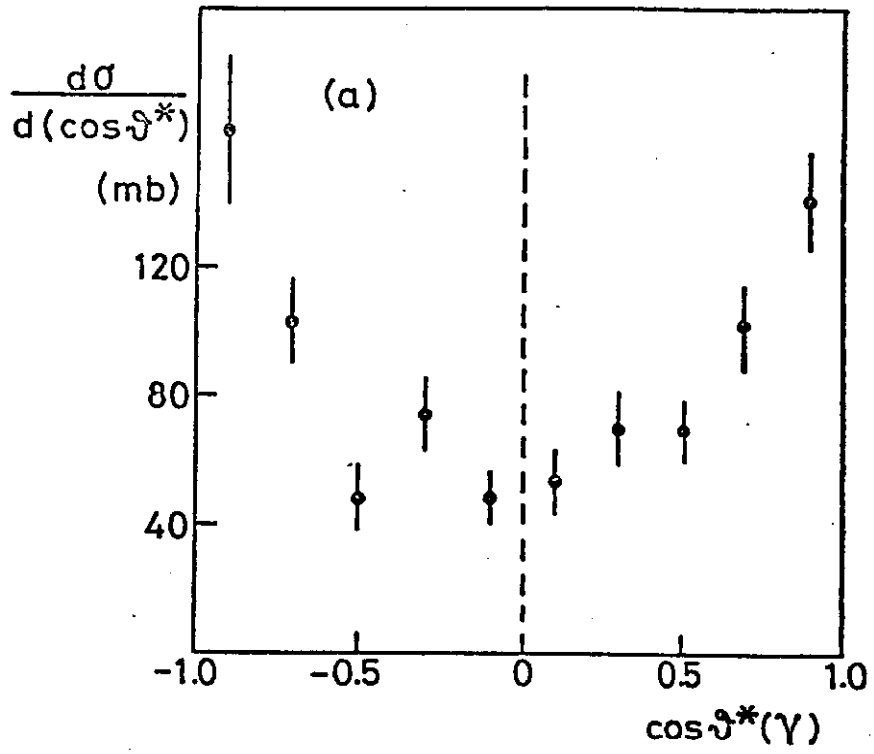
(a)
dσ / d(cos ϑ*)
(mb)
120
80
40
-1.0
-0.5
0
0.5
1.0
cos ϑ*(γ)

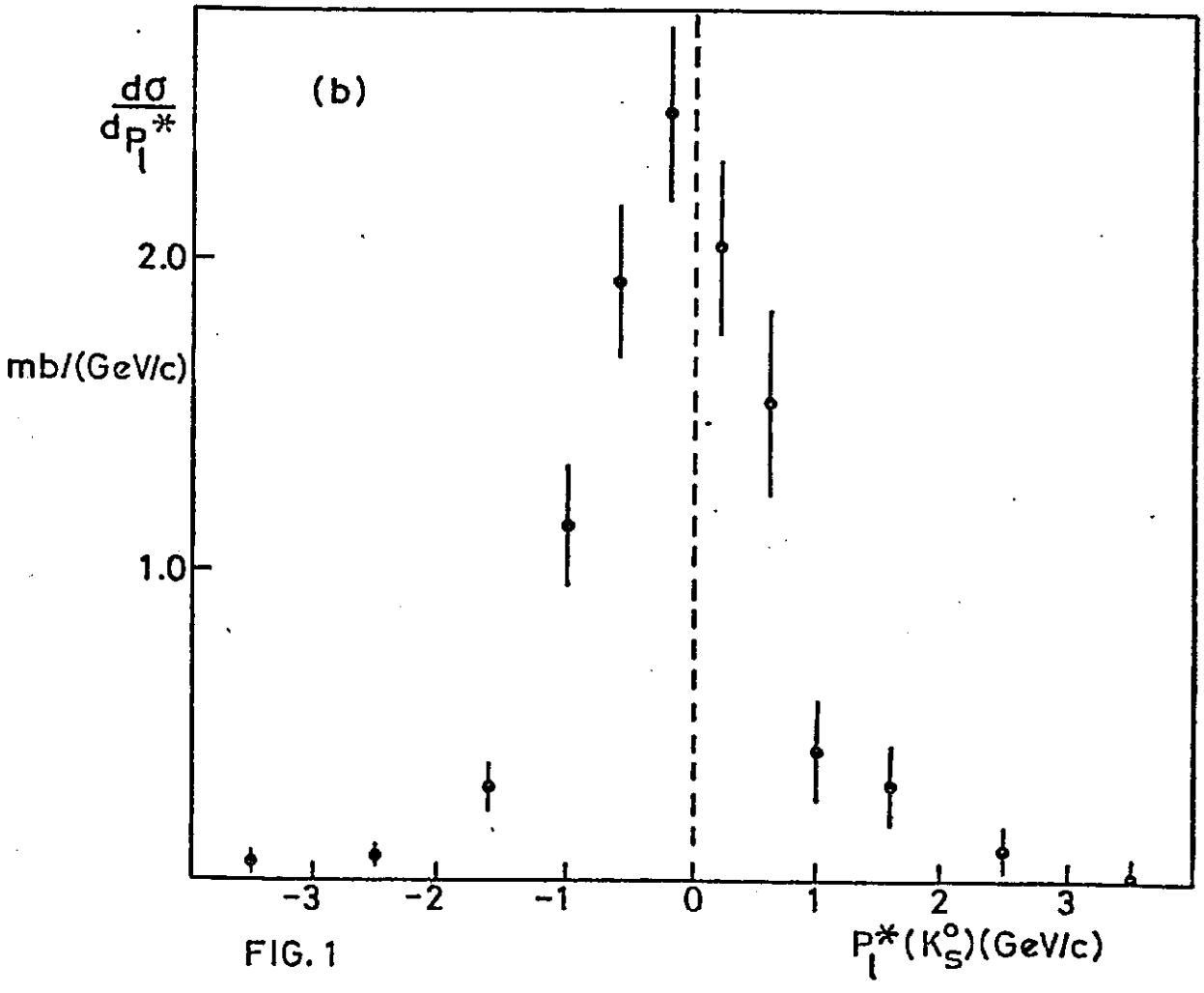
(b)
dσ / dP*l
2.0
mb/(GeV/c)
1.0
-3
-2
-1
0
1
2
3
P*l(K°S)(GeV/c)

FIG. 1

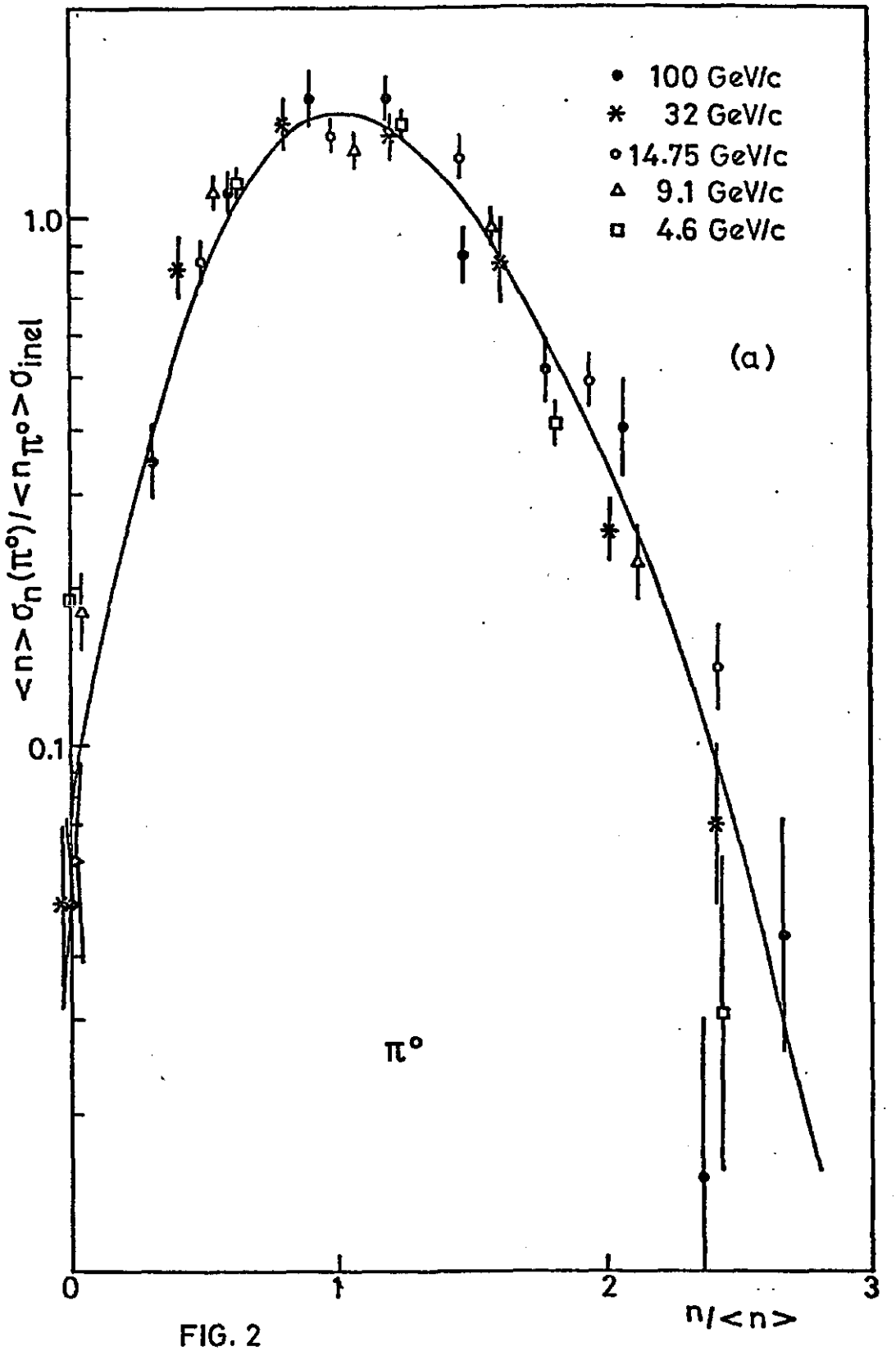
100 GeV/c
32 GeV/c
14.75 GeV/c
9.1 GeV/c
4.6 GeV/c
(a)
1.0
0.1
$\langle n \rangle \sigma_n(\pi^o)/\langle n_{\pi^o} \rangle \sigma_{inel}$
π^o
0
1
2
3
$n/\langle n \rangle$

FIG. 2

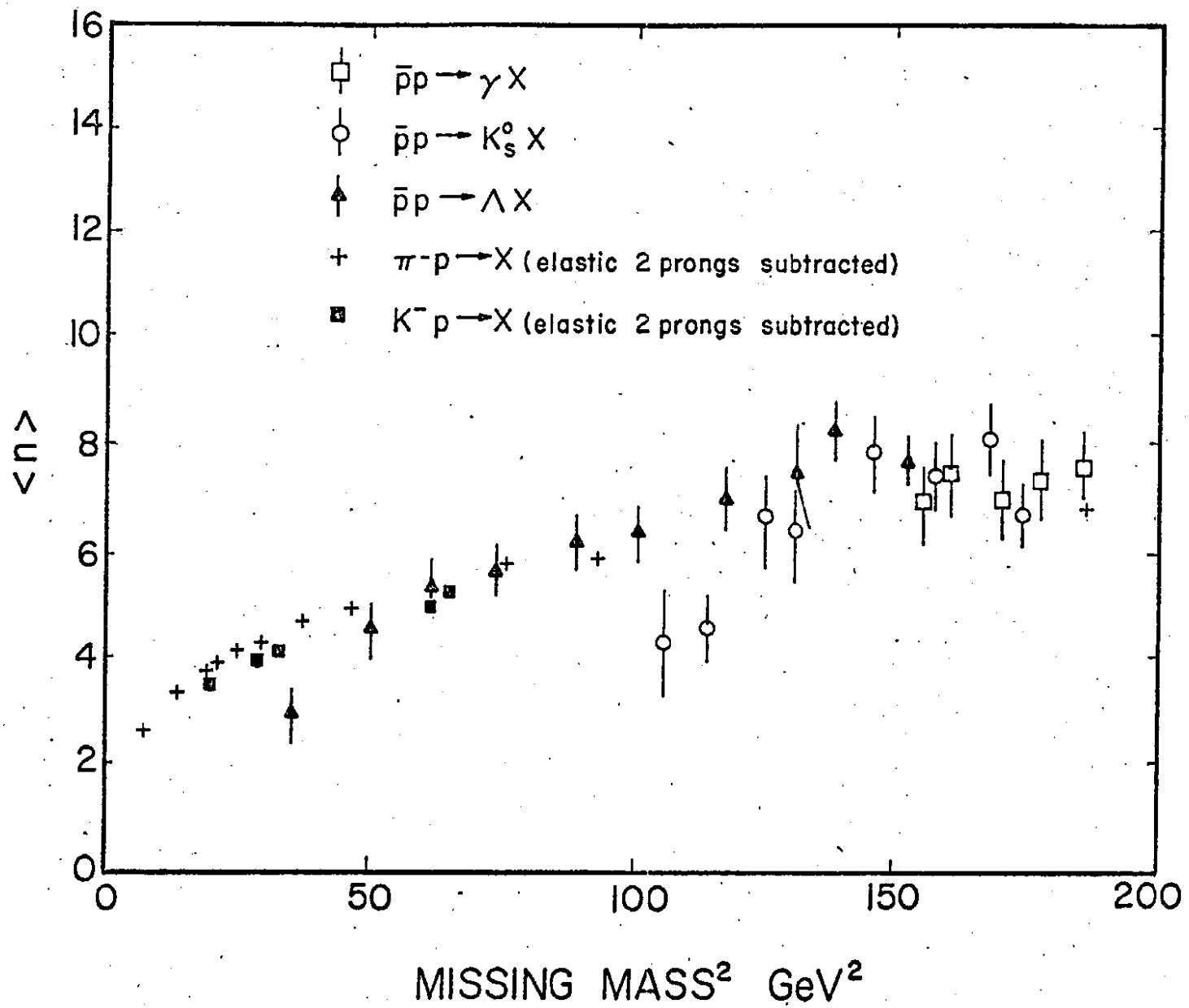
$\bar{p}p \to \gamma X$
$\bar{p}p \to K^0_s X$
$\bar{p}p \to \Lambda X$
$\pi^- p \to X$ (elastic 2 prongs subtracted)
$K^- p \to X$ (elastic 2 prongs subtracted)
$\langle n \rangle$
0
2
4
6
8
10
12
14
16
0
50
100
150
200
MISSING MASS^2 GeV^2

Fig. 11

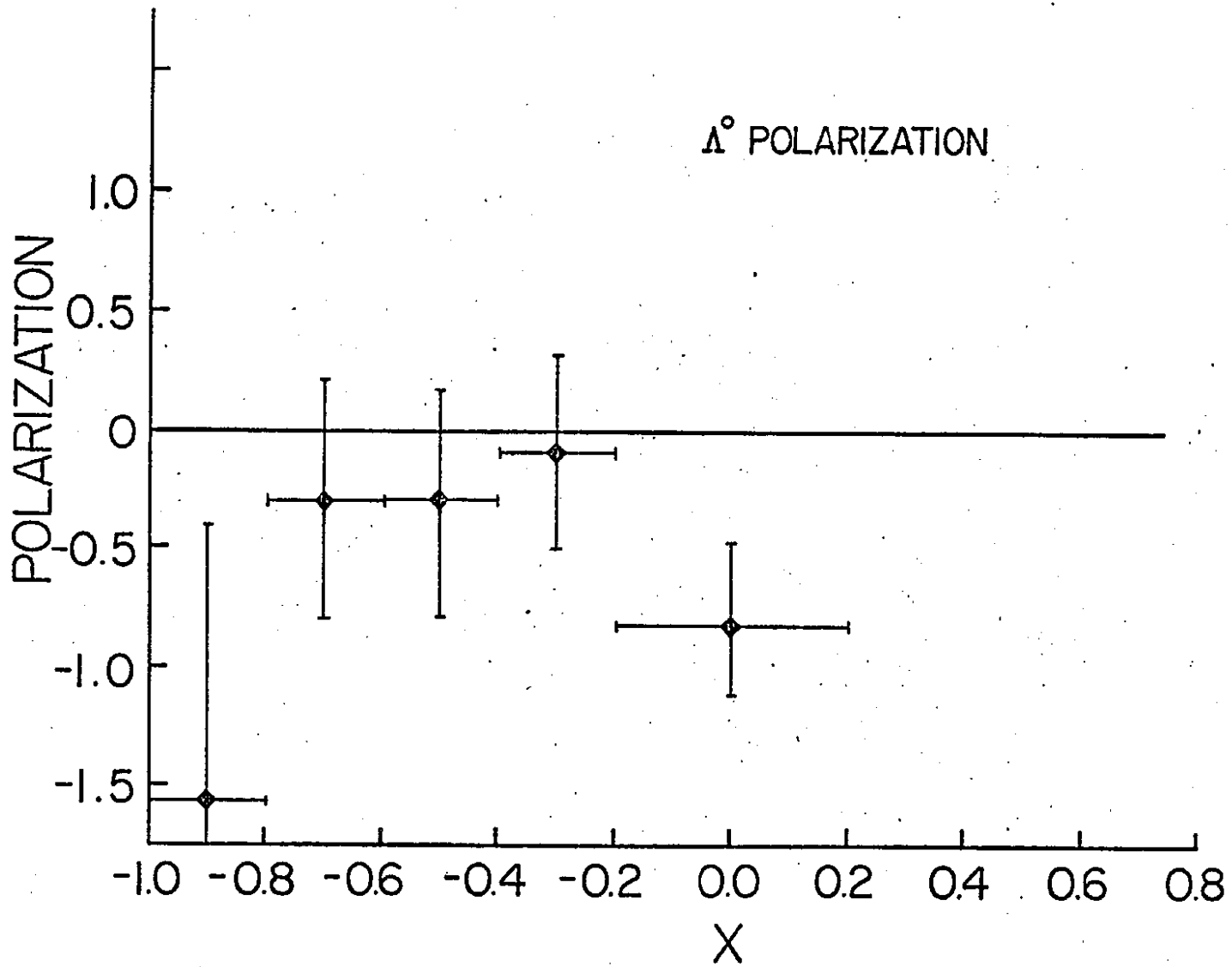
Λ° POLARIZATION
POLARIZATION
1.0
0.5
0
-0.5
-1.0
-1.5
-1.0
-0.8
-0.6
-0.4
-0.2
0.0
0.2
0.4
0.6
0.8
X

Fig. 12

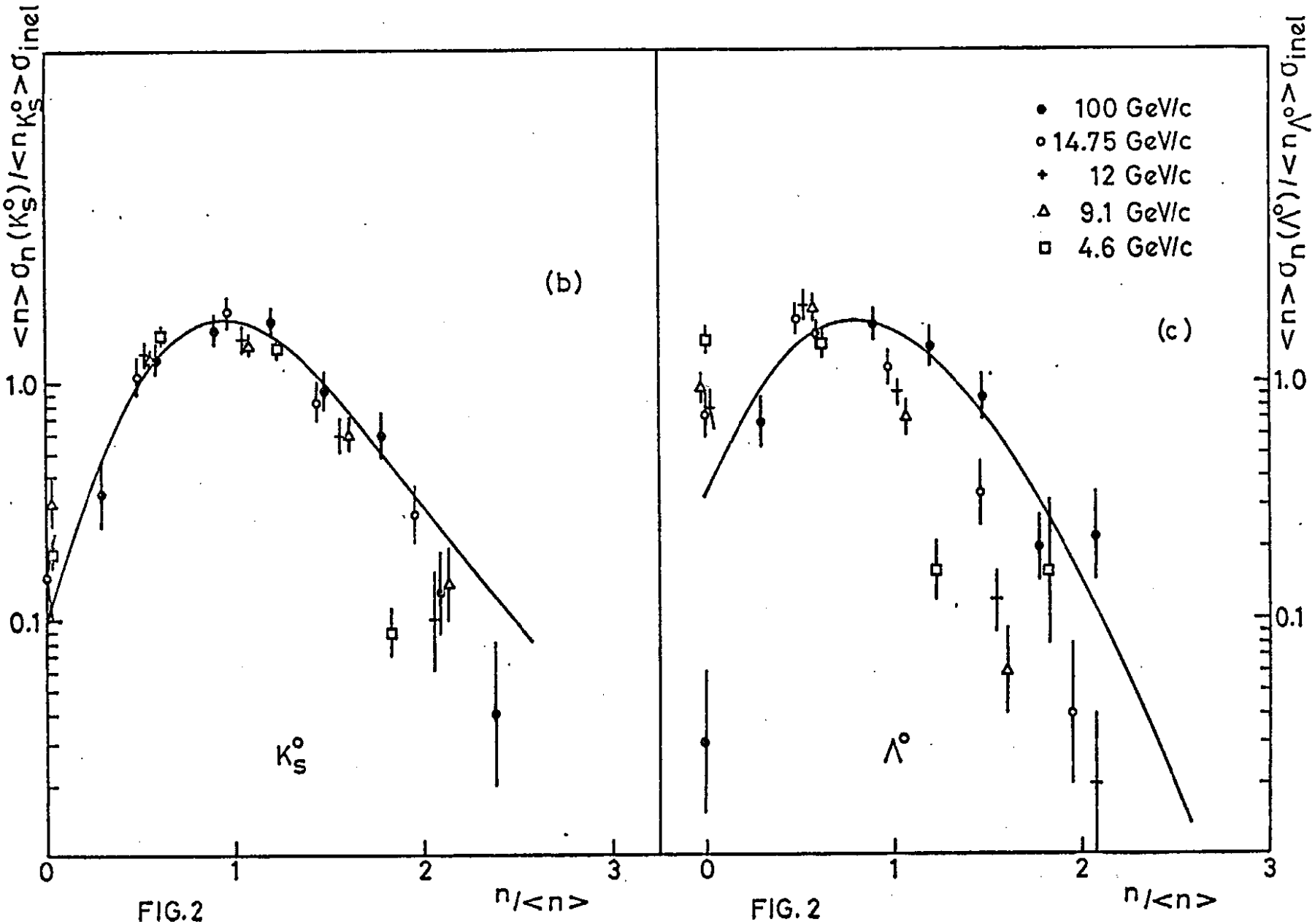
$<n>\sigma_n(K_s^o)/<n_{K_s^o}>\sigma_{inel}$
(b)
K_s^o
1.0
0.1
0
1
2
3
$n/<n>$
$<n>\sigma_n(\Lambda^o)/<n_{\Lambda^o}>\sigma_{inel}$
100 GeV/c
14.75 GeV/c
12 GeV/c
9.1 GeV/c
4.6 GeV/c
(c)
Λ^o
1.0
0.1
0
1
2
3
$n/<n>$

FIG.2

FIG. 2

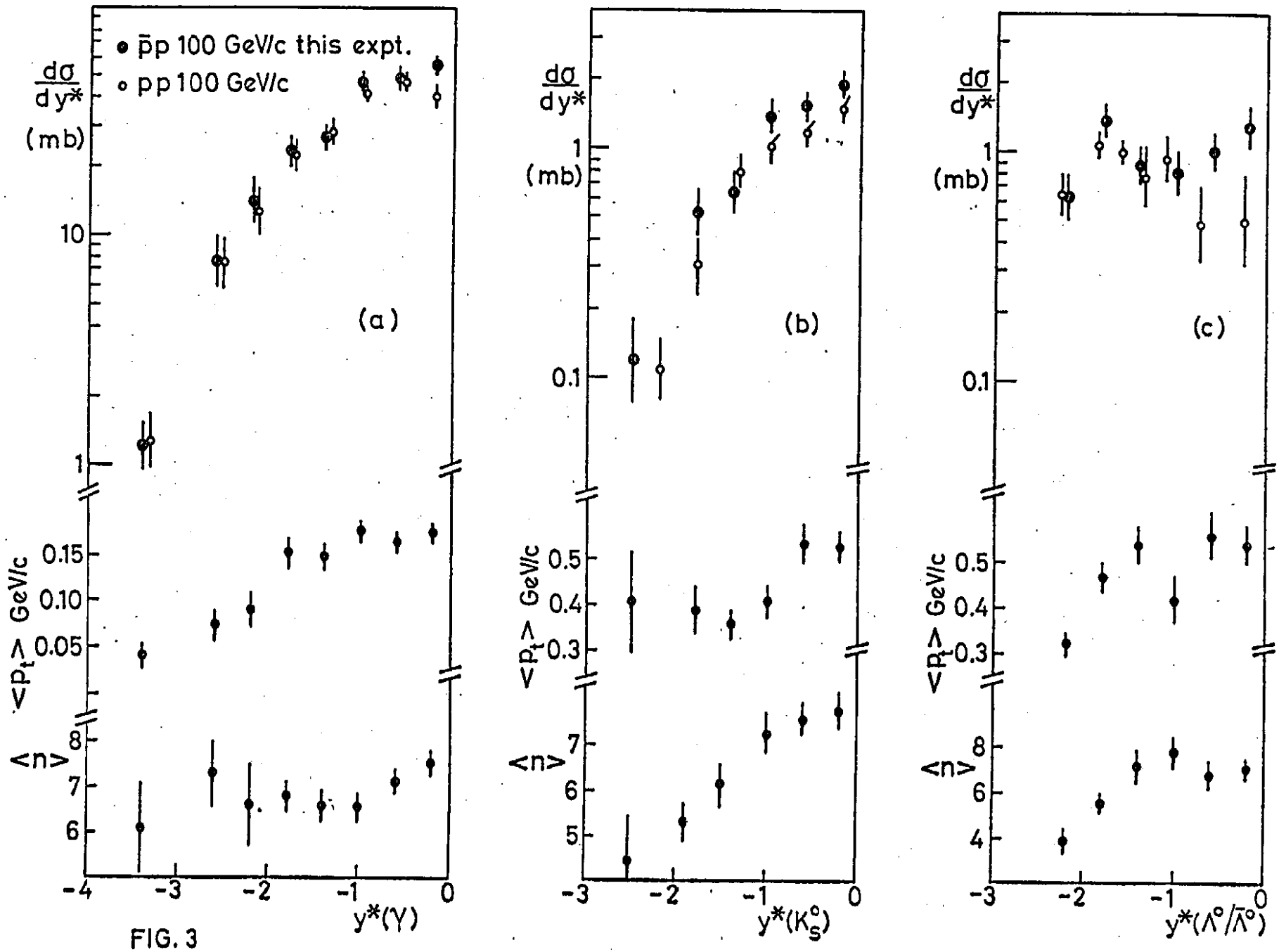
● p̄p 100 GeV/c this expt.
○ pp 100 GeV/c
dσ/dy* (mb)
(a)
(b)
(c)
<p_t> GeV/c
<n>
y*(γ)
y*(K°_S)
y*(Λ°/Λ̄°)

FIG. 3

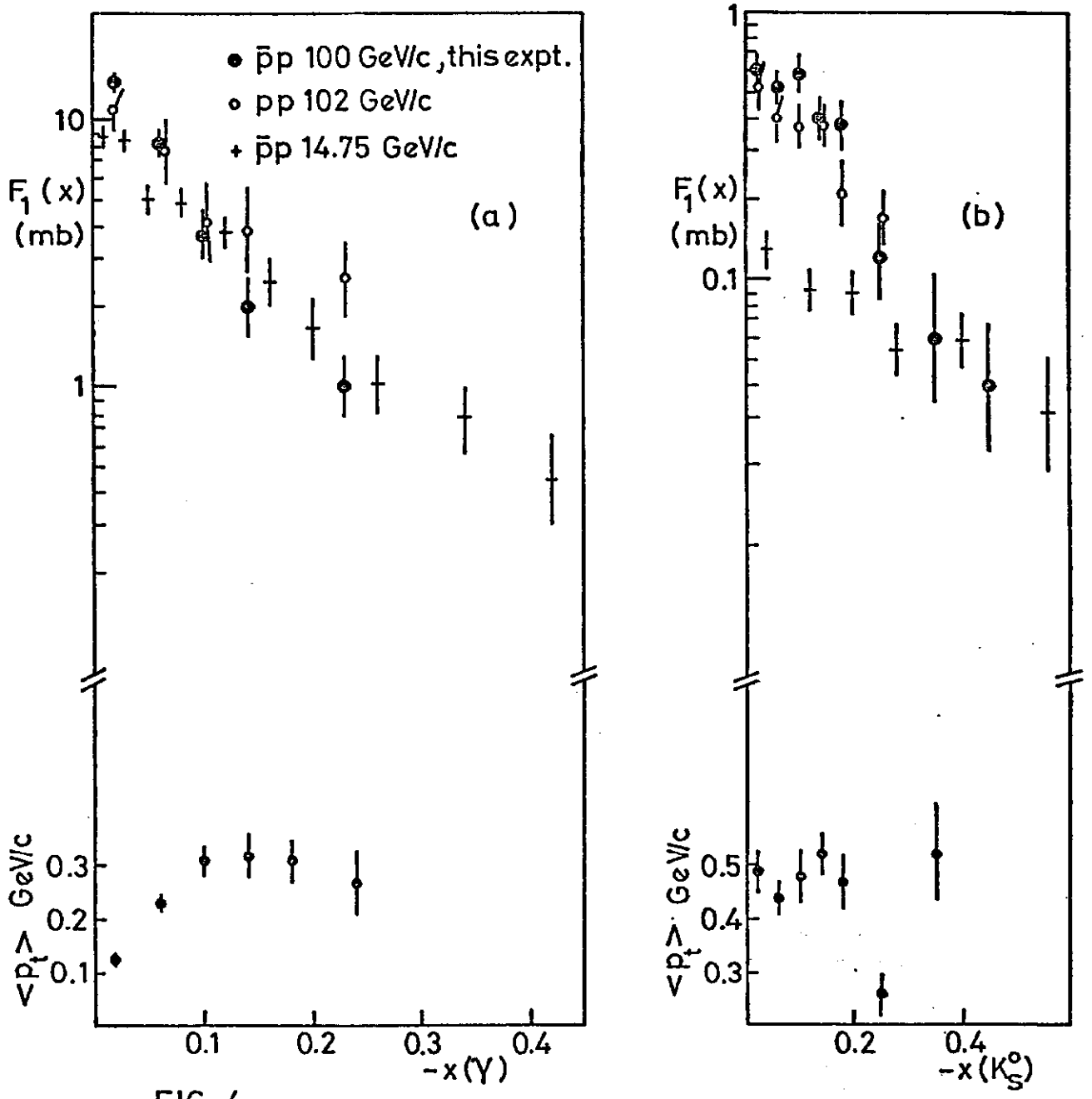
p̄p 100 GeV/c, this expt.
pp 102 GeV/c
p̄p 14.75 GeV/c
(a)
(b)
$F_1(x)$ (mb)
$\langle p_t \rangle$ GeV/c
$-x(\gamma)$
$-x(K^0_S)$

FIG. 4

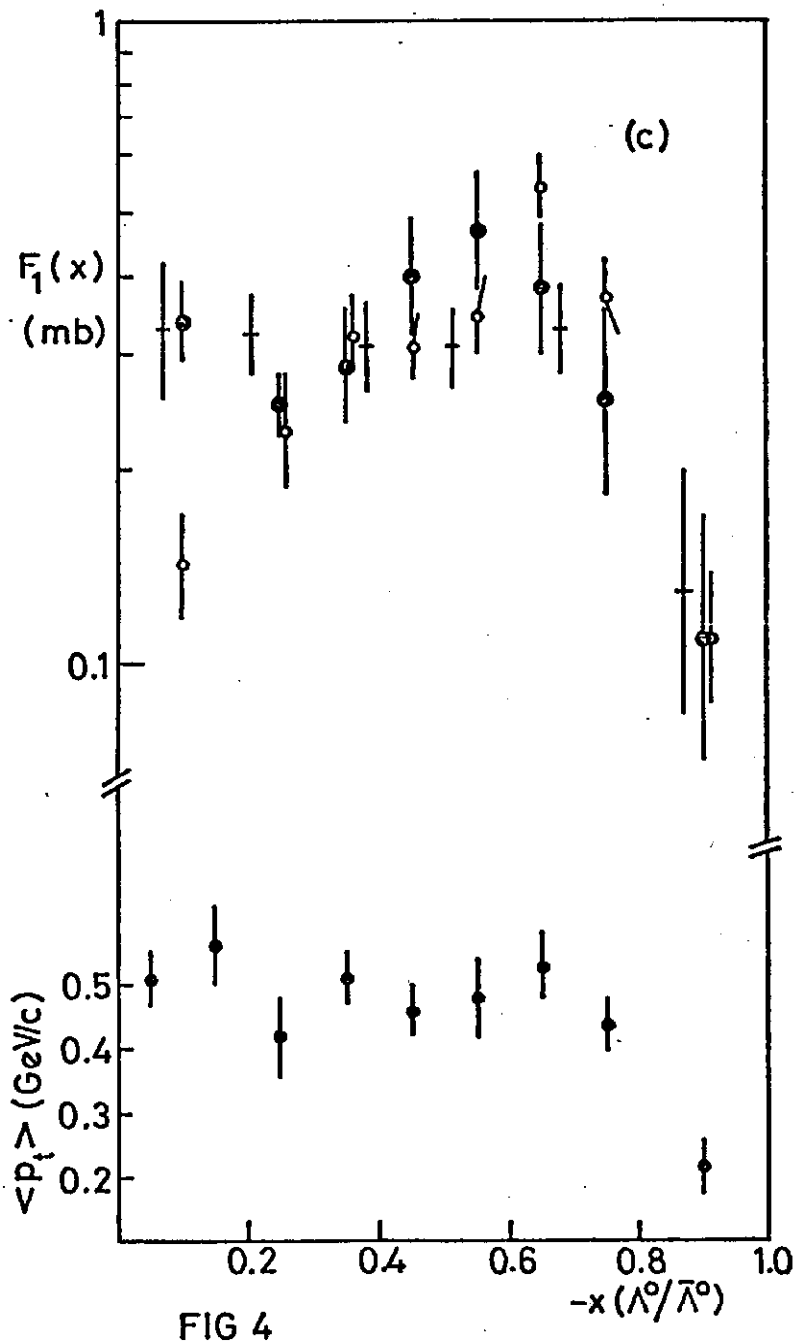
1
(c)
$F_1(x)$
(mb)
0.1
0.5
0.4
0.3
0.2
$\langle p_t \rangle$ (GeV/c)
0.2
0.4
0.6
0.8
1.0
$-x\ (\Lambda^0/\bar{\Lambda}^0)$

FIG 4

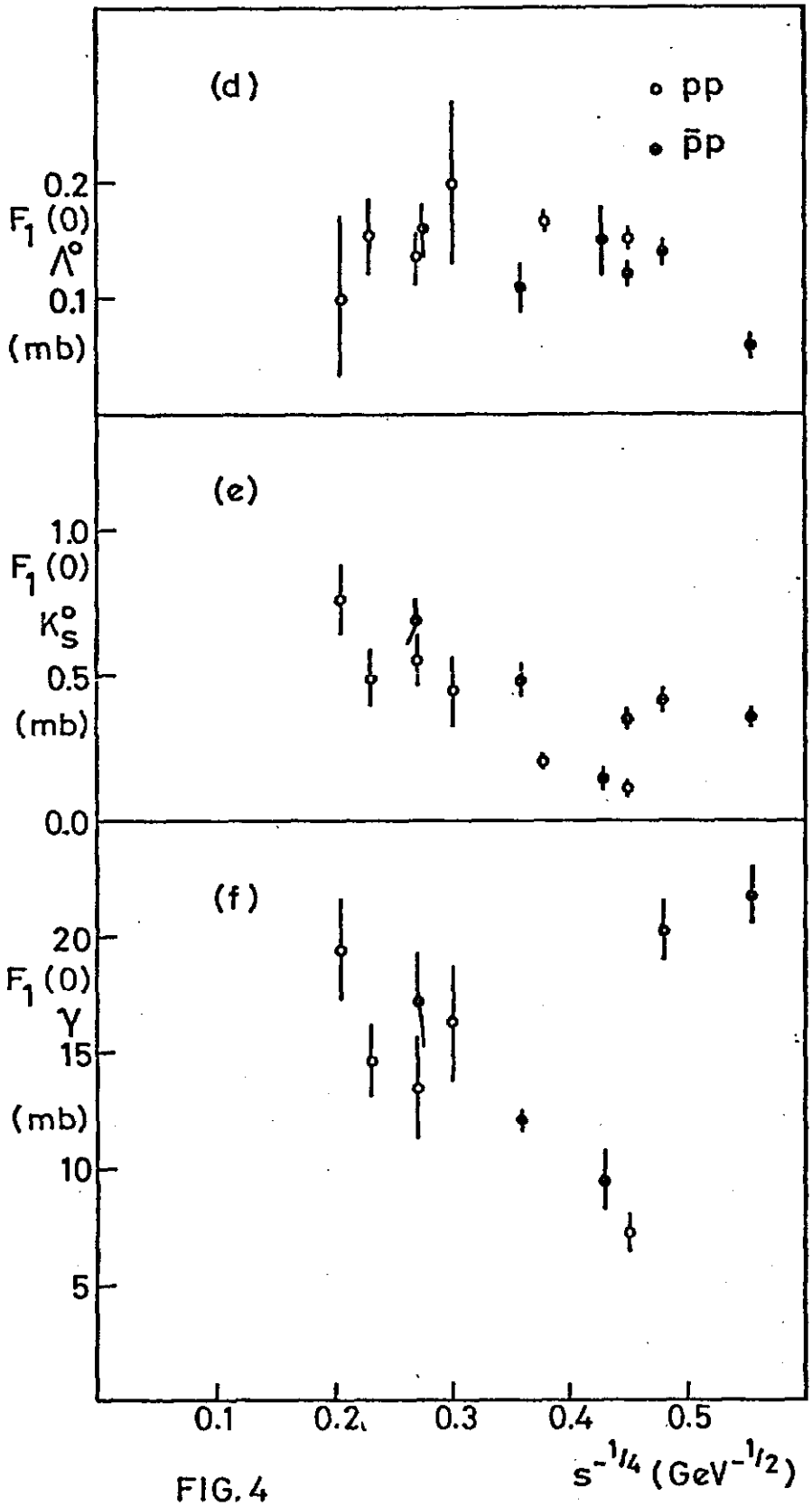
(d)
pp
p̄p
0.2
$F_1(0)$
Λ^o
0.1
(mb)
(e)
1.0
$F_1(0)$
K_s^o
0.5
(mb)
0.0
(f)
20
$F_1(0)$
γ
15
(mb)
10
5
0.1
0.2
0.3
0.4
0.5
$s^{-1/4}$ ($GeV^{-1/2}$)

FIG. 4

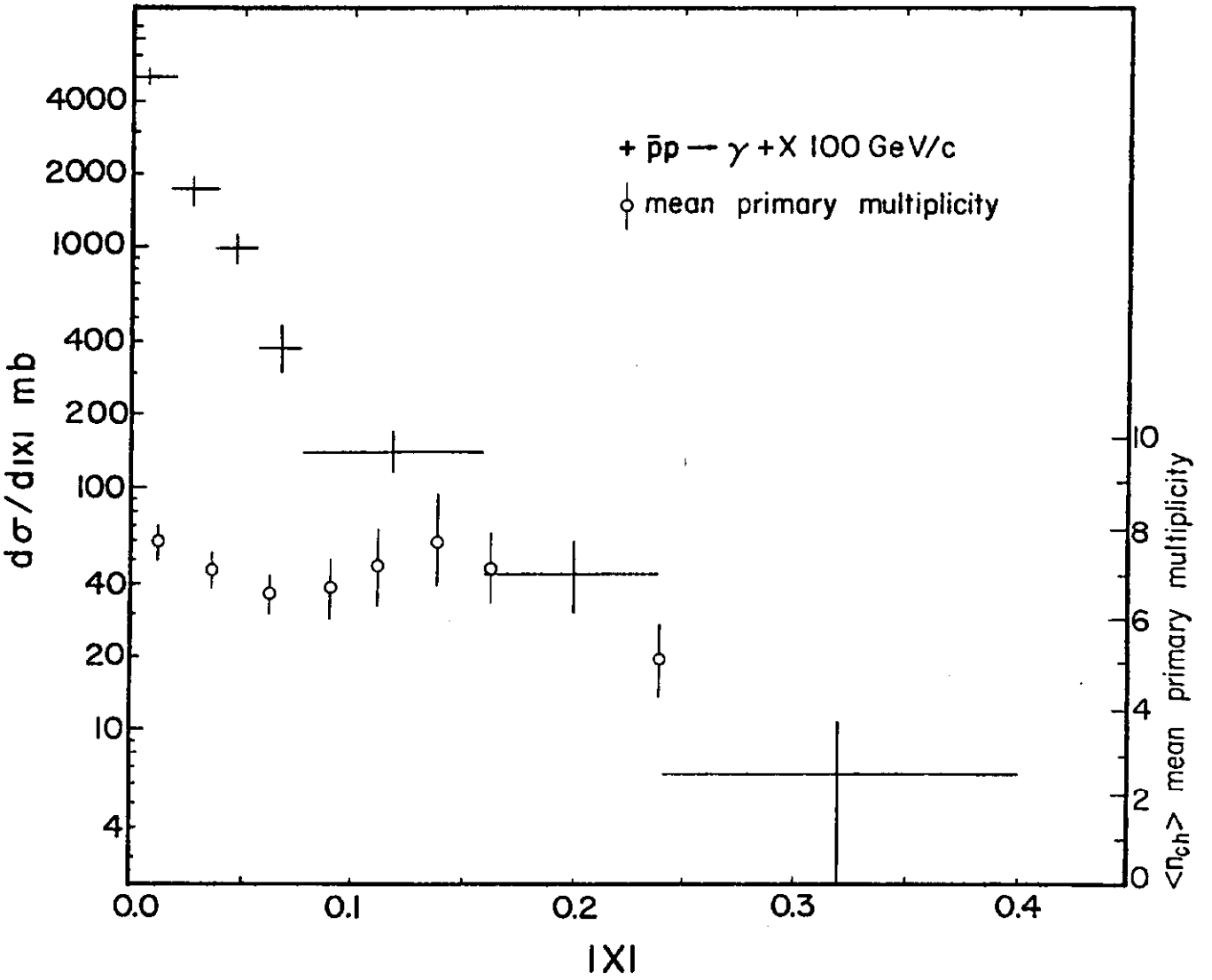
+ p̄p → γ + X 100 GeV/c
mean primary multiplicity
dσ/d|x| mb
<n_ch> mean primary multiplicity
|X|
4000
2000
1000
400
200
100
40
20
10
4
0.0
0.1
0.2
0.3
0.4
10
8
6
4
2
0

Fig.5(a)

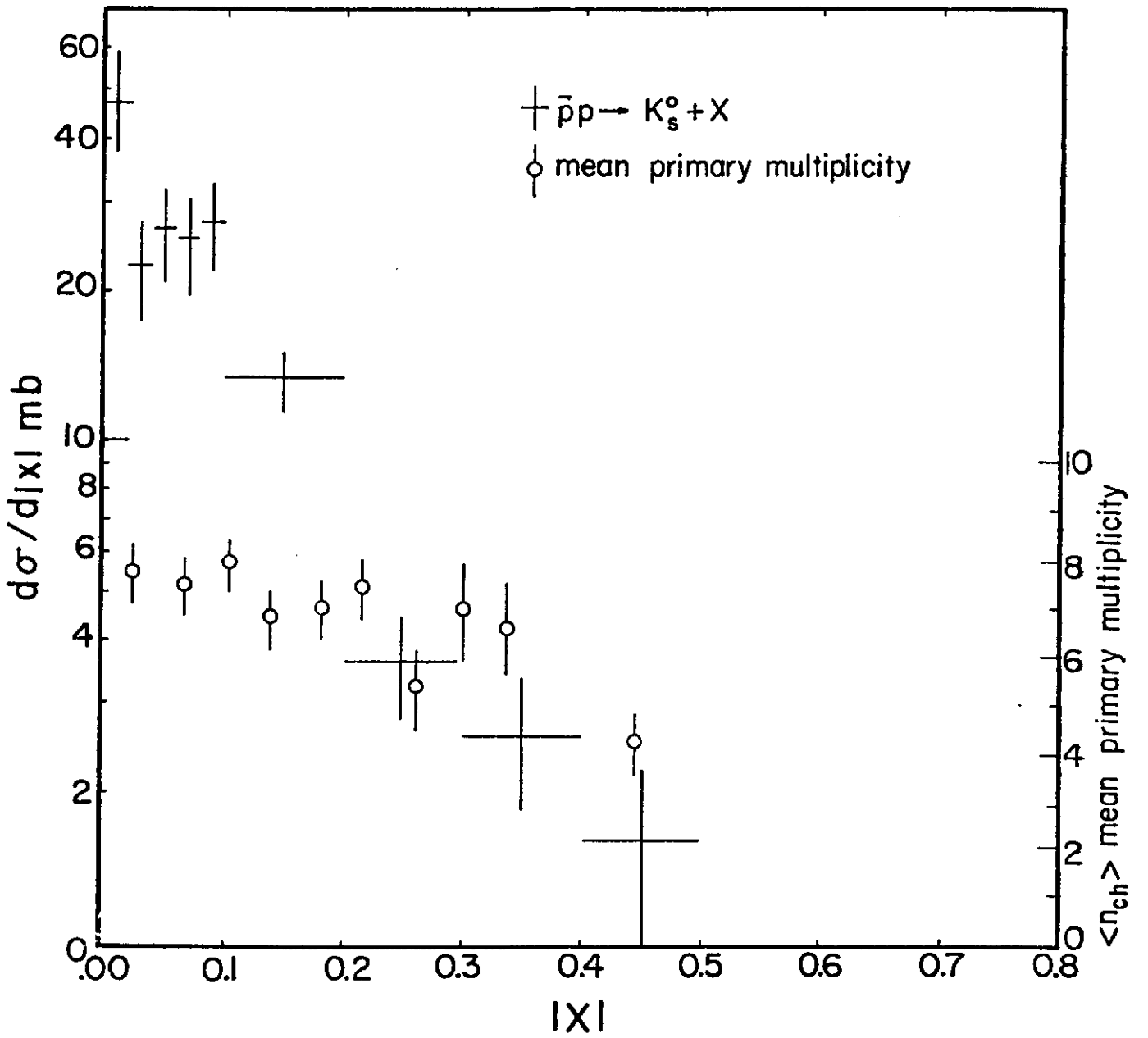
$\bar{p}p \rightarrow K^0_s + X$
mean primary multiplicity
$d\sigma/d|x|$ mb
$\langle n_{ch} \rangle$ mean primary multiplicity
$|X|$
60
40
20
10
8
6
4
2
0
.00
0.1
0.2
0.3
0.4
0.5
0.6
0.7
0.8

Fig. 5(b)

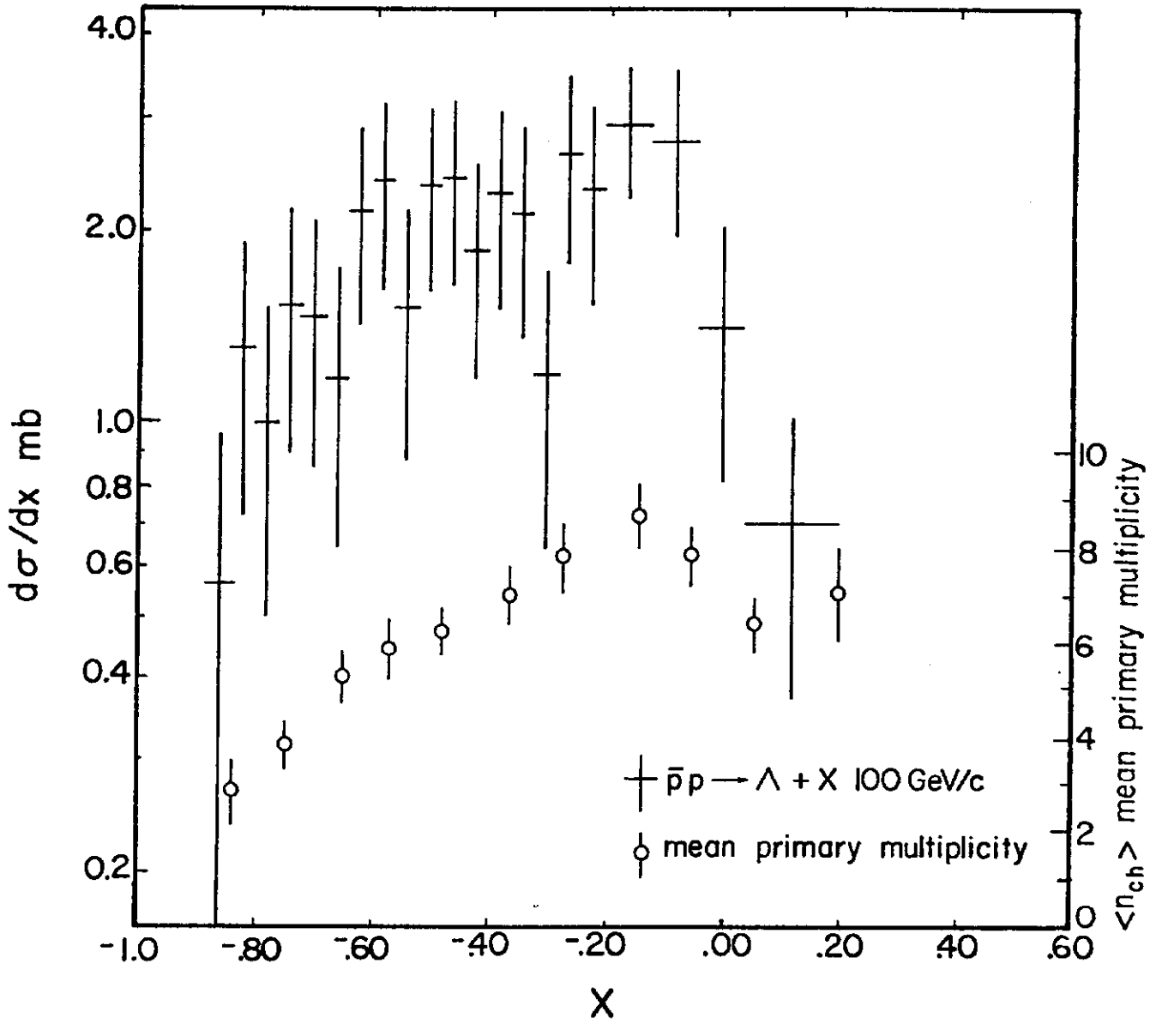
4.0
2.0
1.0
0.8
0.6
0.4
0.2
dσ/dx mb
-1.0
-.80
-.60
-.40
-.20
.00
.20
.40
.60
X
10
8
6
4
2
0
<n_ch> mean primary multiplicity
p̄p → Λ + X 100 GeV/c
mean primary multiplicity

Fig. 5(c)

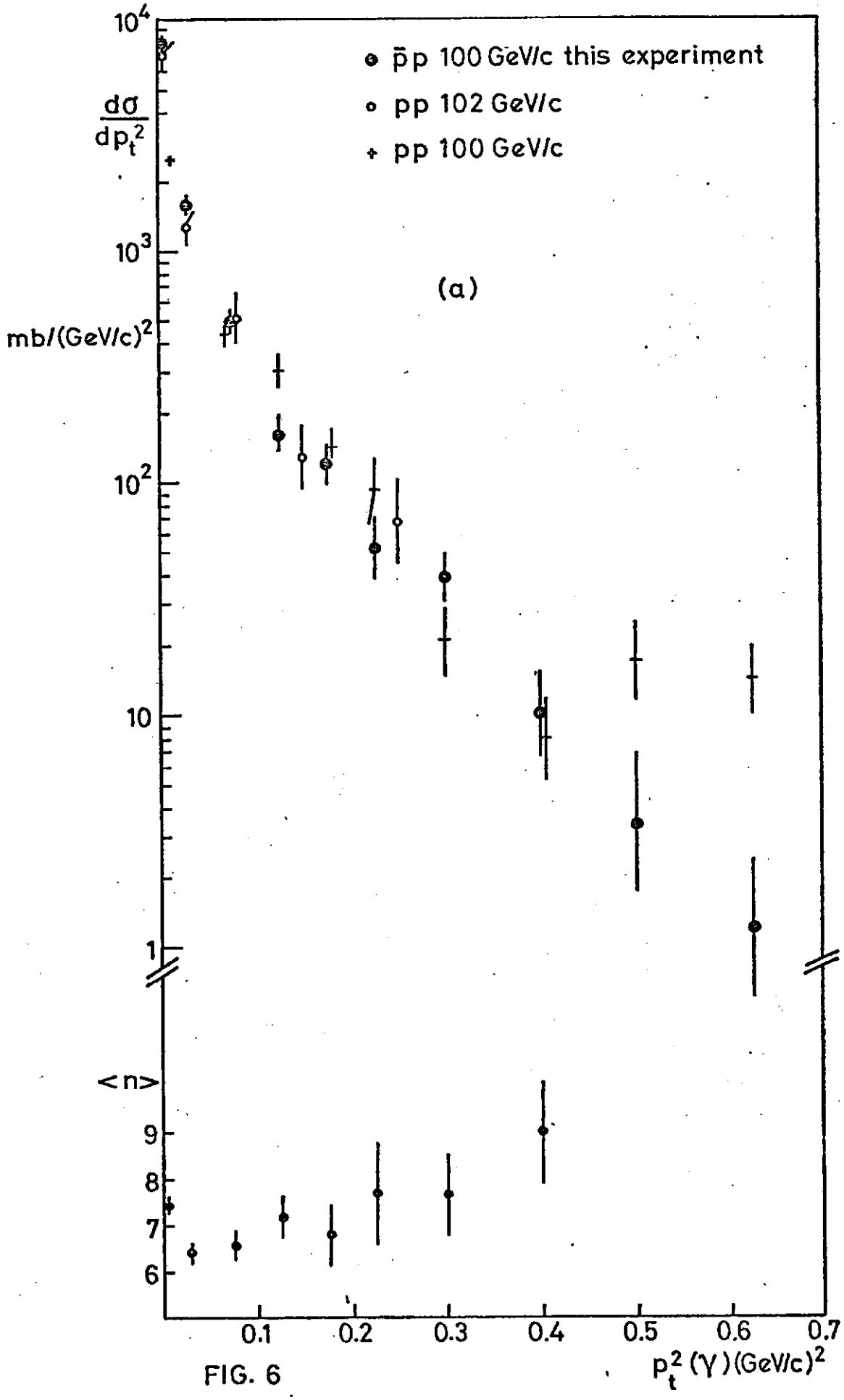
$\bar{p}p$ 100 GeV/c this experiment
pp 102 GeV/c
pp 100 GeV/c
(a)
$\frac{d\sigma}{dp_t^2}$
mb/(GeV/c)^2
10^4
10^3
10^2
10
1
<n>
9
8
7
6
0.1
0.2
0.3
0.4
0.5
0.6
0.7
p_t^2 (γ) (GeV/c)^2

FIG. 6

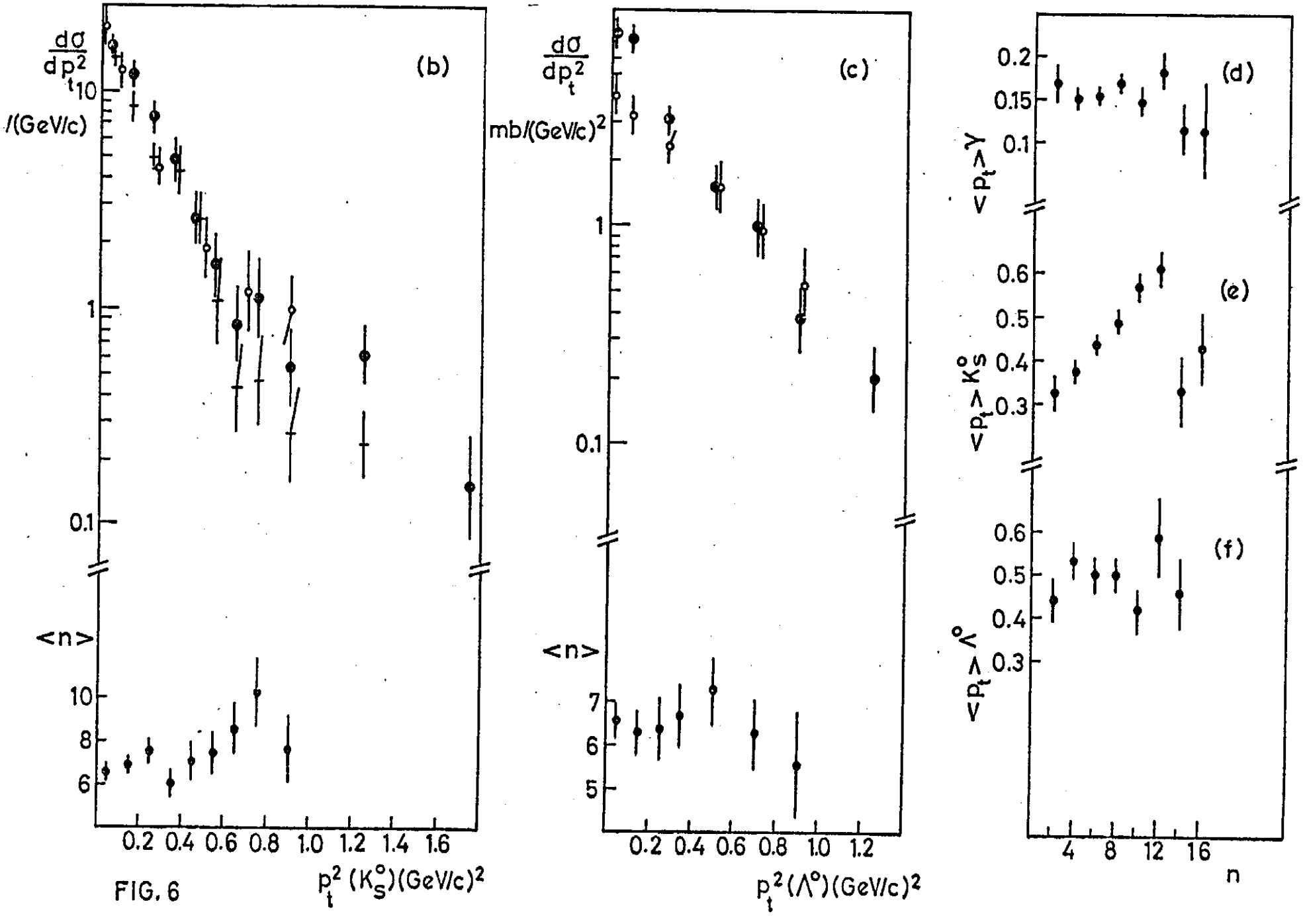
(b)
(c)
(d)
(e)
(f)
$\frac{d\sigma}{dp_t^2}$ /(GeV/c)
$\frac{d\sigma}{dp_t^2}$ mb/(GeV/c)^2
<n>
p_t^2 (K_S^o)(GeV/c)^2
p_t^2(Λ^o)(GeV/c)^2
<p_t>$^\gamma$
<p_t>K_S^o
<p_t>Λ^o
n

FIG. 6

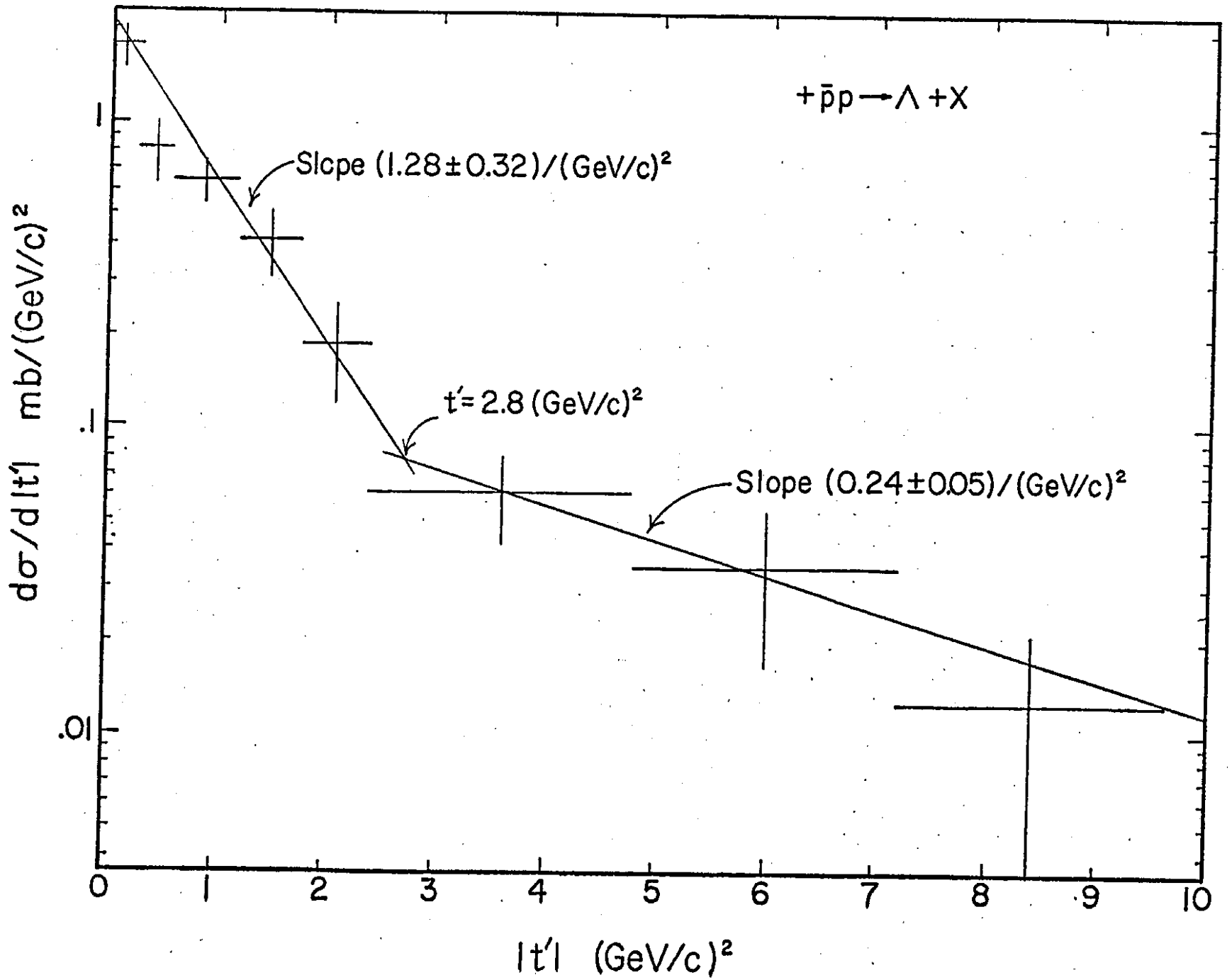
+p̄p→Λ+X
Slope (1.28±0.32)/(GeV/c)²
t′= 2.8 (GeV/c)²
Slope (0.24±0.05)/(GeV/c)²
dσ/d|t′| mb/(GeV/c)²
1
.1
.01
0
1
2
3
4
5
6
7
8
9
10
|t′| (GeV/c)²

Fig. 7

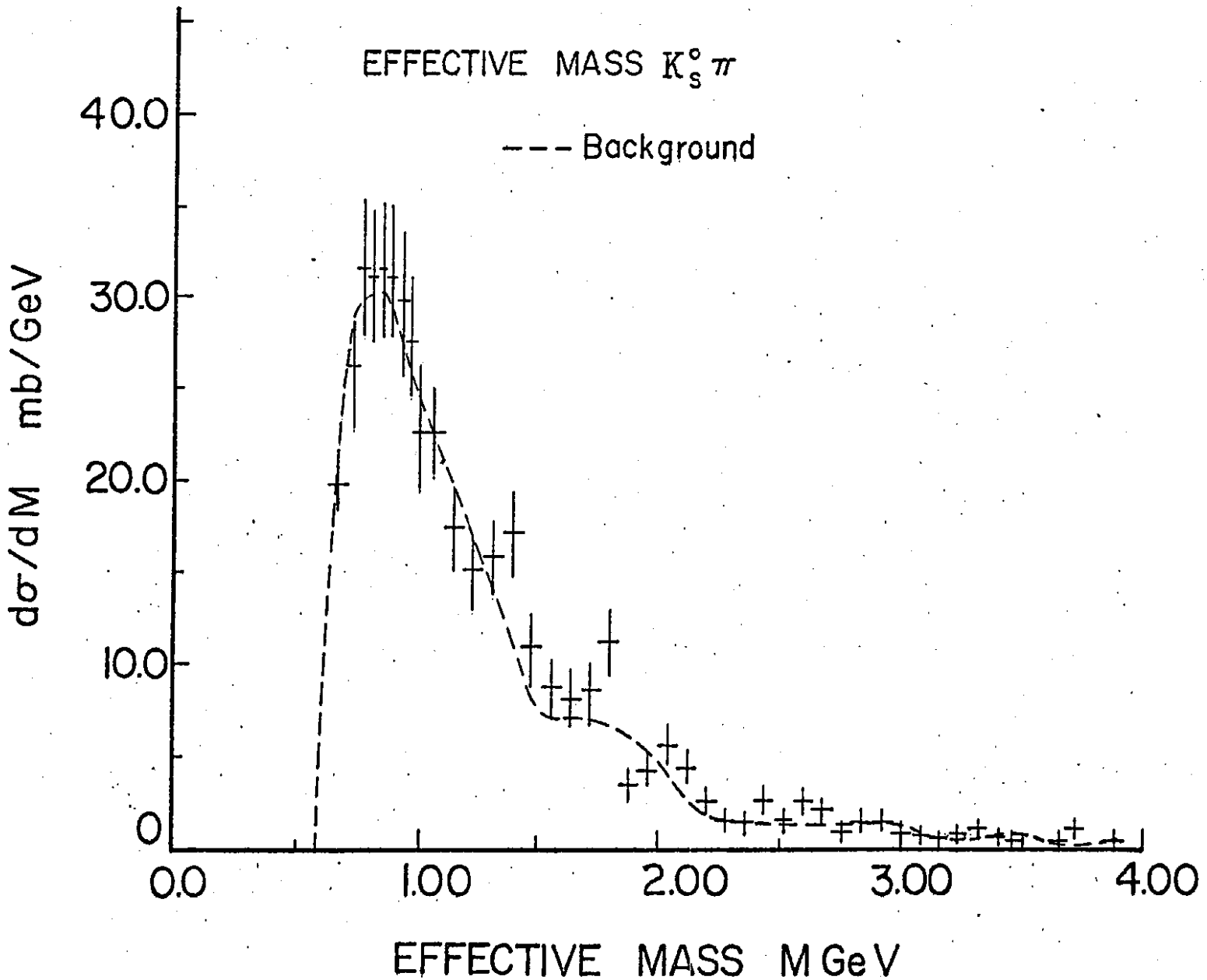
EFFECTIVE MASS $K_s^0 \pi$
--- Background
40.0
30.0
20.0
10.0
0
dσ/dM mb/GeV
0.0
1.00
2.00
3.00
4.00
EFFECTIVE MASS M GeV

Fig. 8 (a)

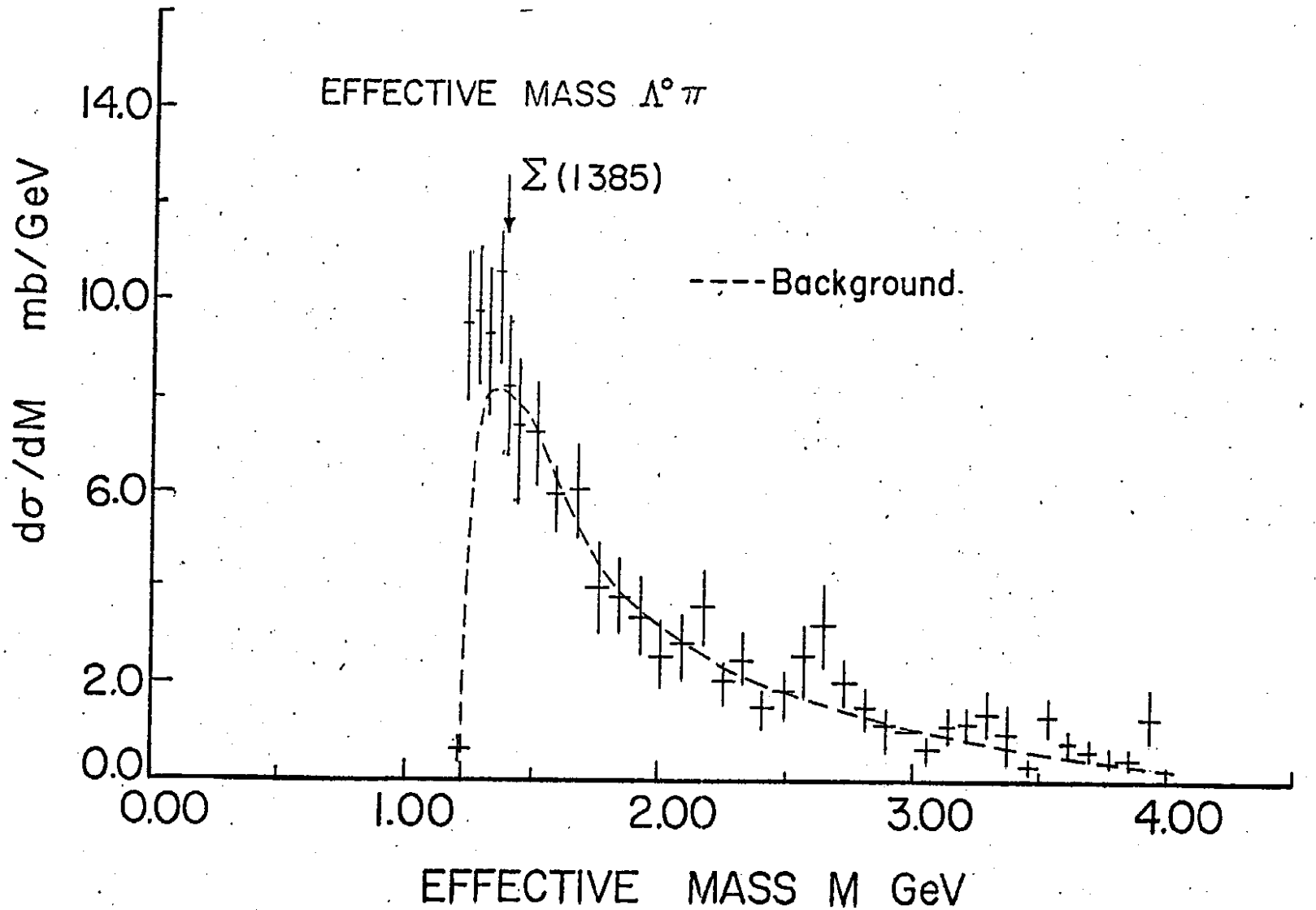
EFFECTIVE MASS $\Lambda^\circ \pi$
Σ(1385)
Background.
14.0
10.0
6.0
2.0
0.0
$d\sigma/dM$ mb/GeV
0.00
1.00
2.00
3.00
4.00
EFFECTIVE MASS M GeV

Fig. 8(b)

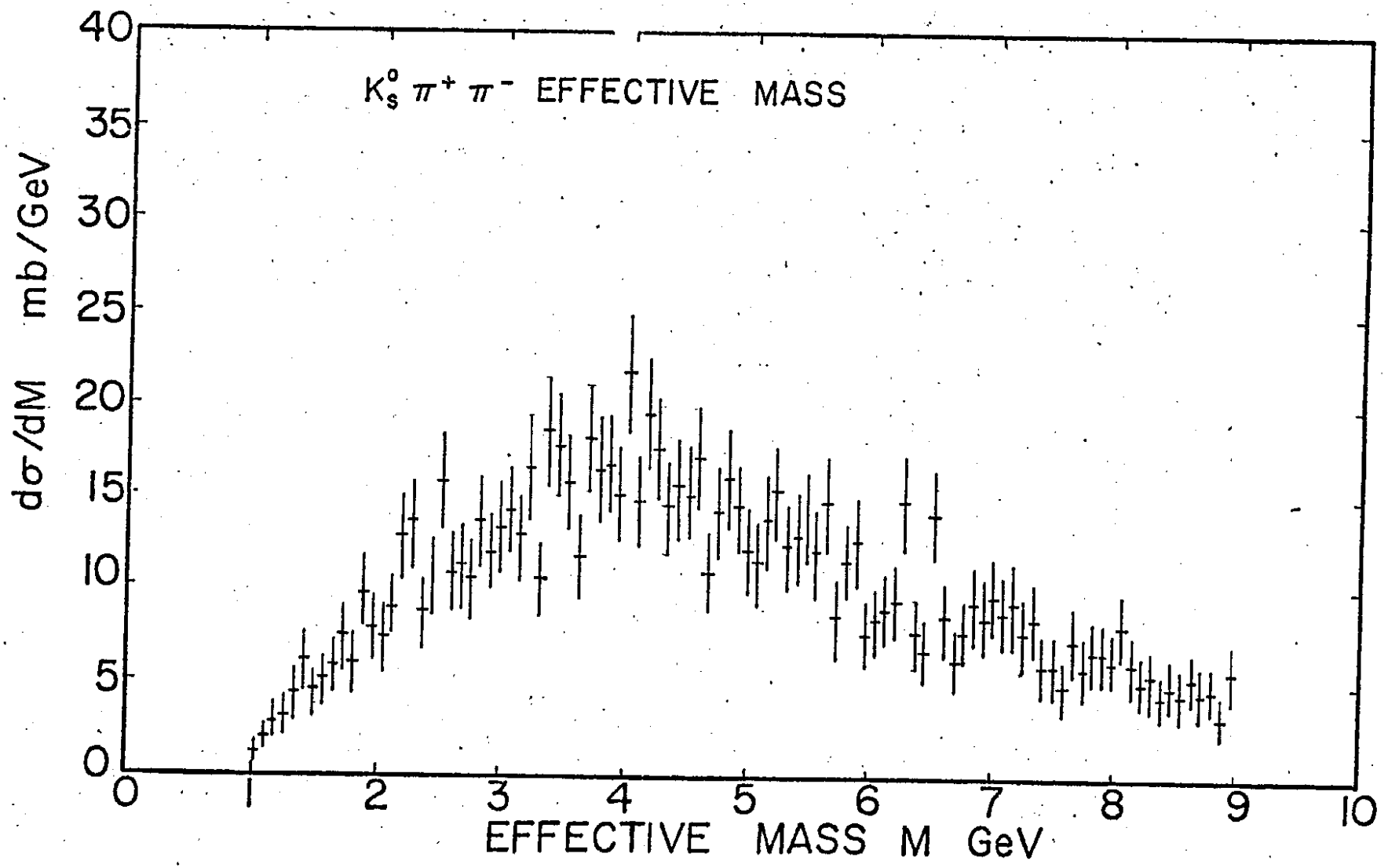
$K_s^0 \pi^+ \pi^-$ EFFECTIVE MASS
$d\sigma/dM$ mb/GeV
0
5
10
15
20
25
30
35
40
0
1
2
3
4
5
6
7
8
9
10
EFFECTIVE MASS M GeV

Fig. 9(a)

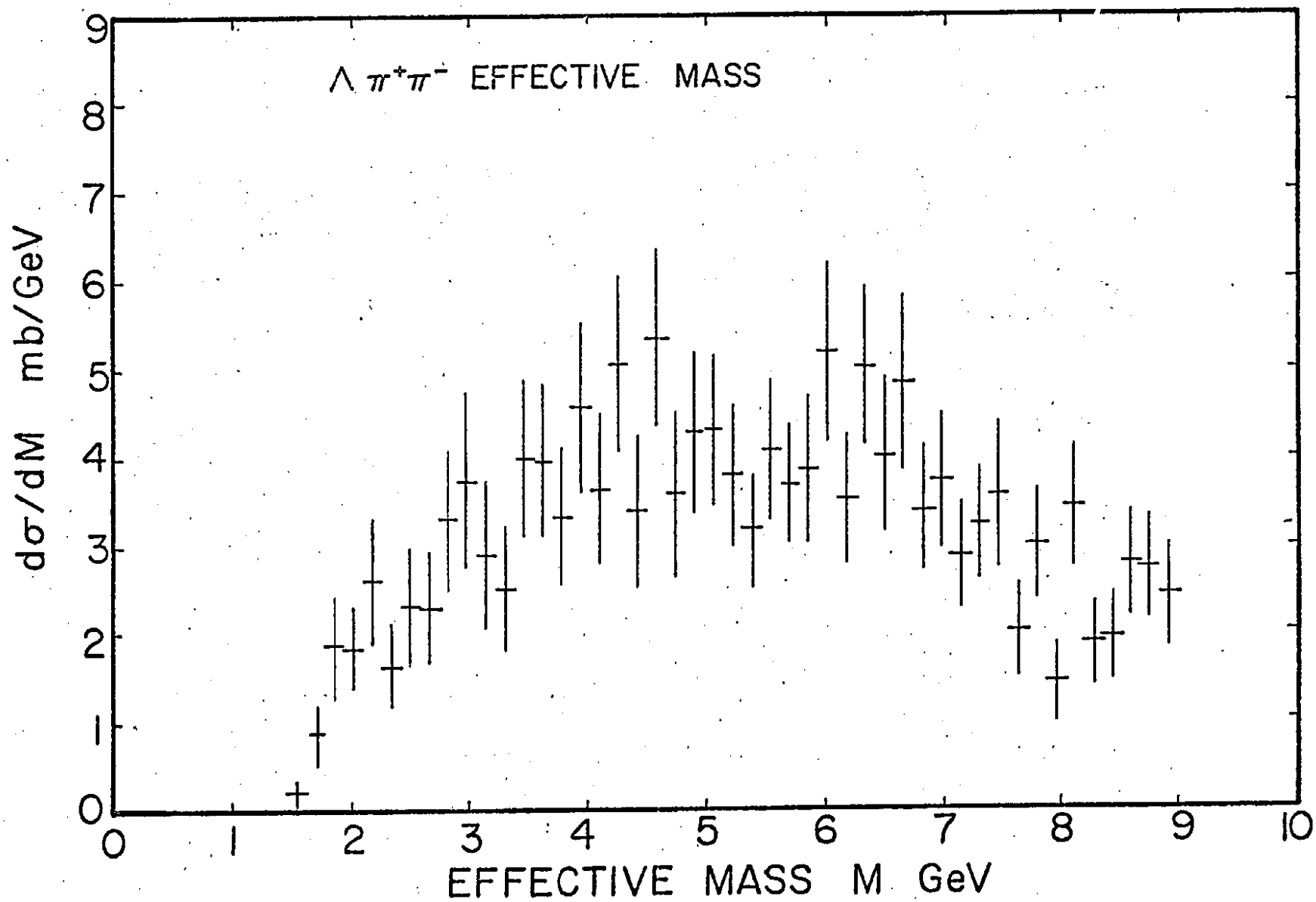
Λ π⁺π⁻ EFFECTIVE MASS
dσ/dM mb/GeV
EFFECTIVE MASS M GeV
0
1
2
3
4
5
6
7
8
9
10

Fig. 9(b)

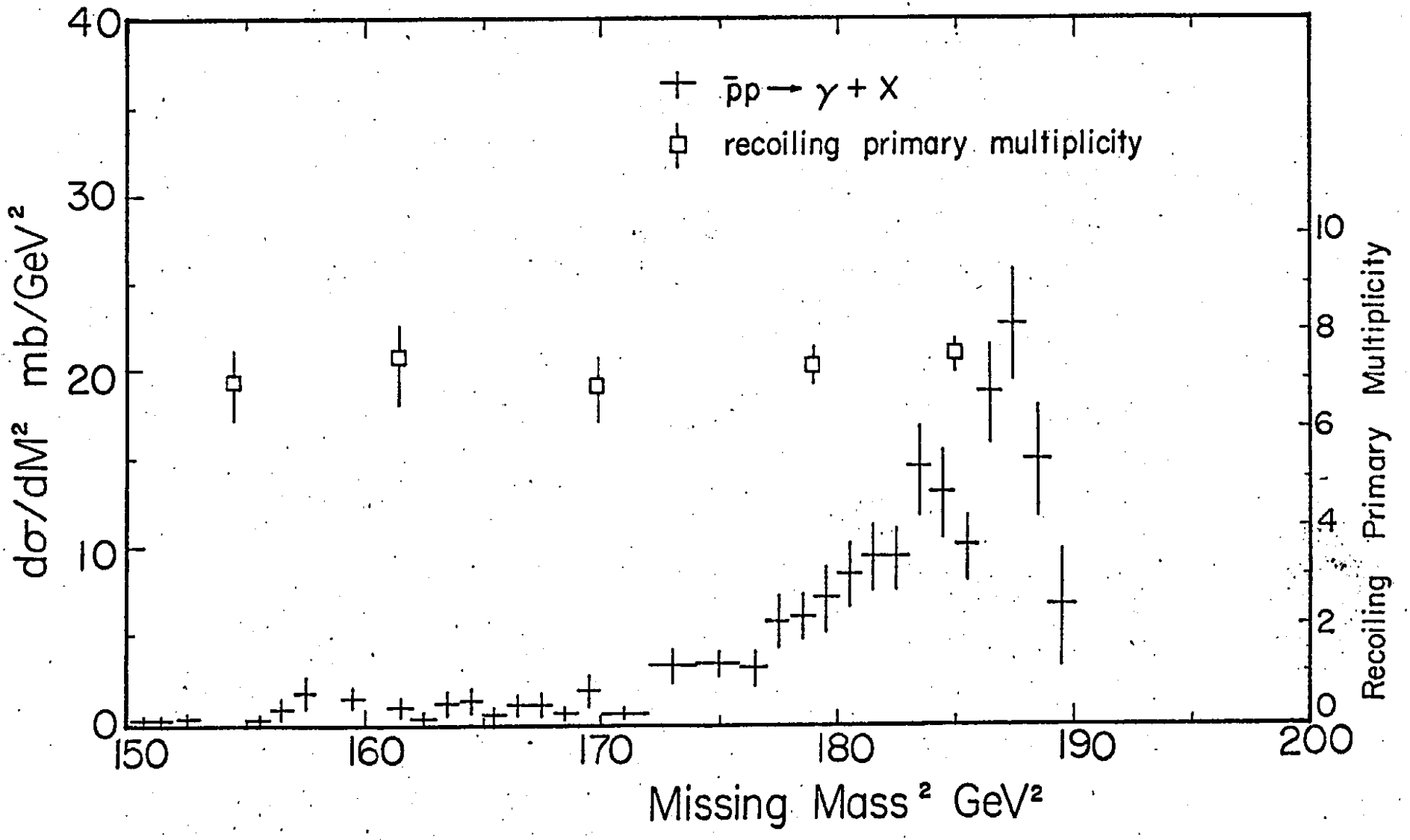
$\bar{p}p \rightarrow \gamma + X$
recoiling primary multiplicity
$d\sigma/dM^2$ mb/GeV^2
Recoiling Primary Multiplicity
Missing Mass^2 GeV^2
0
10
20
30
40
150
160
170
180
190
200
0
2
4
6
8
10

Fig. 10(a)

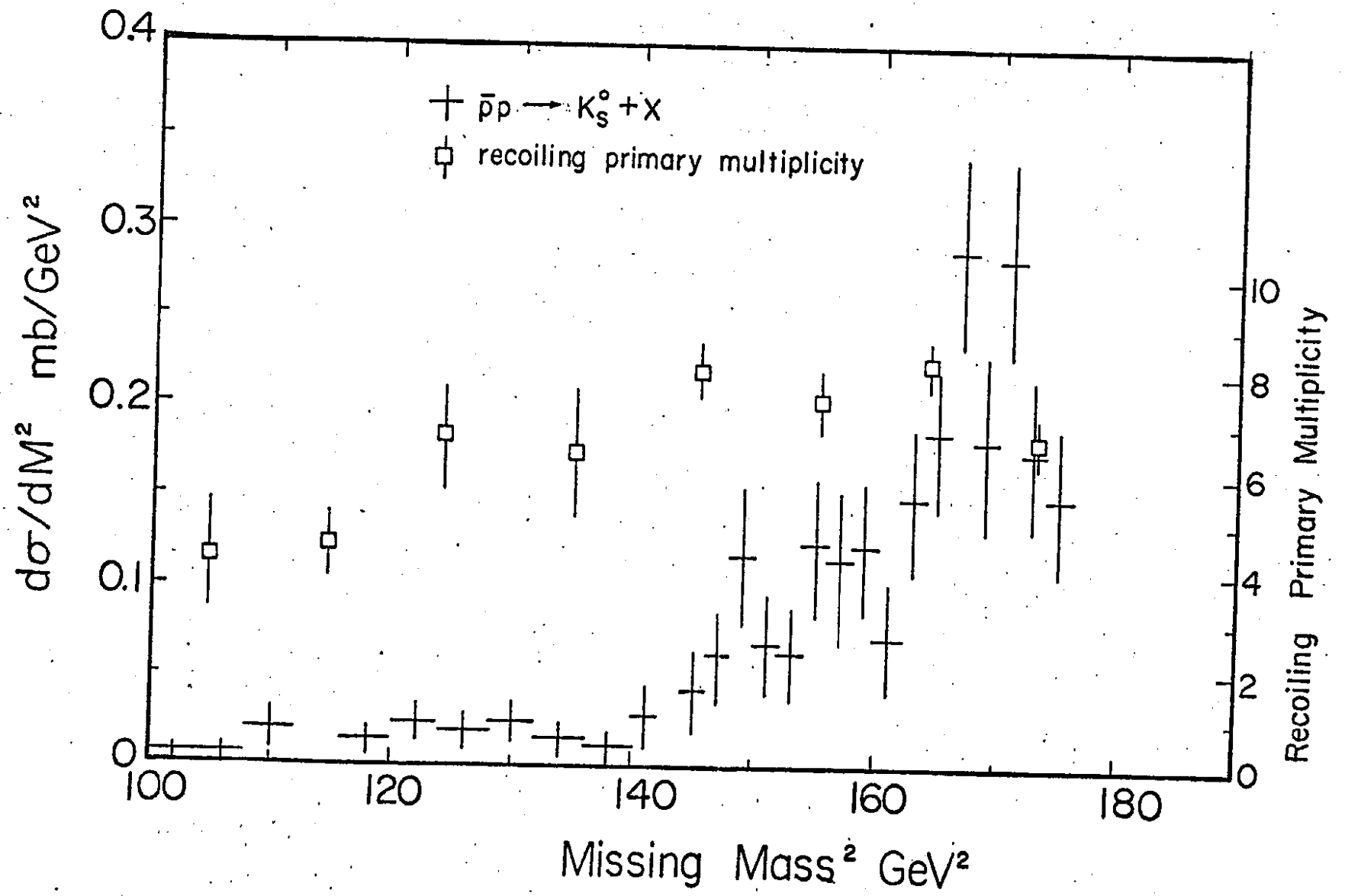
$\bar{p}p \rightarrow K_s^0 + X$
recoiling primary multiplicity
$d\sigma/dM^2$ mb/GeV^2
Recoiling Primary Multiplicity
Missing Mass^2 GeV^2
0.4
0.3
0.2
0.1
0
100
120
140
160
180
10
8
6
4
2
0

Fig. 10(b)

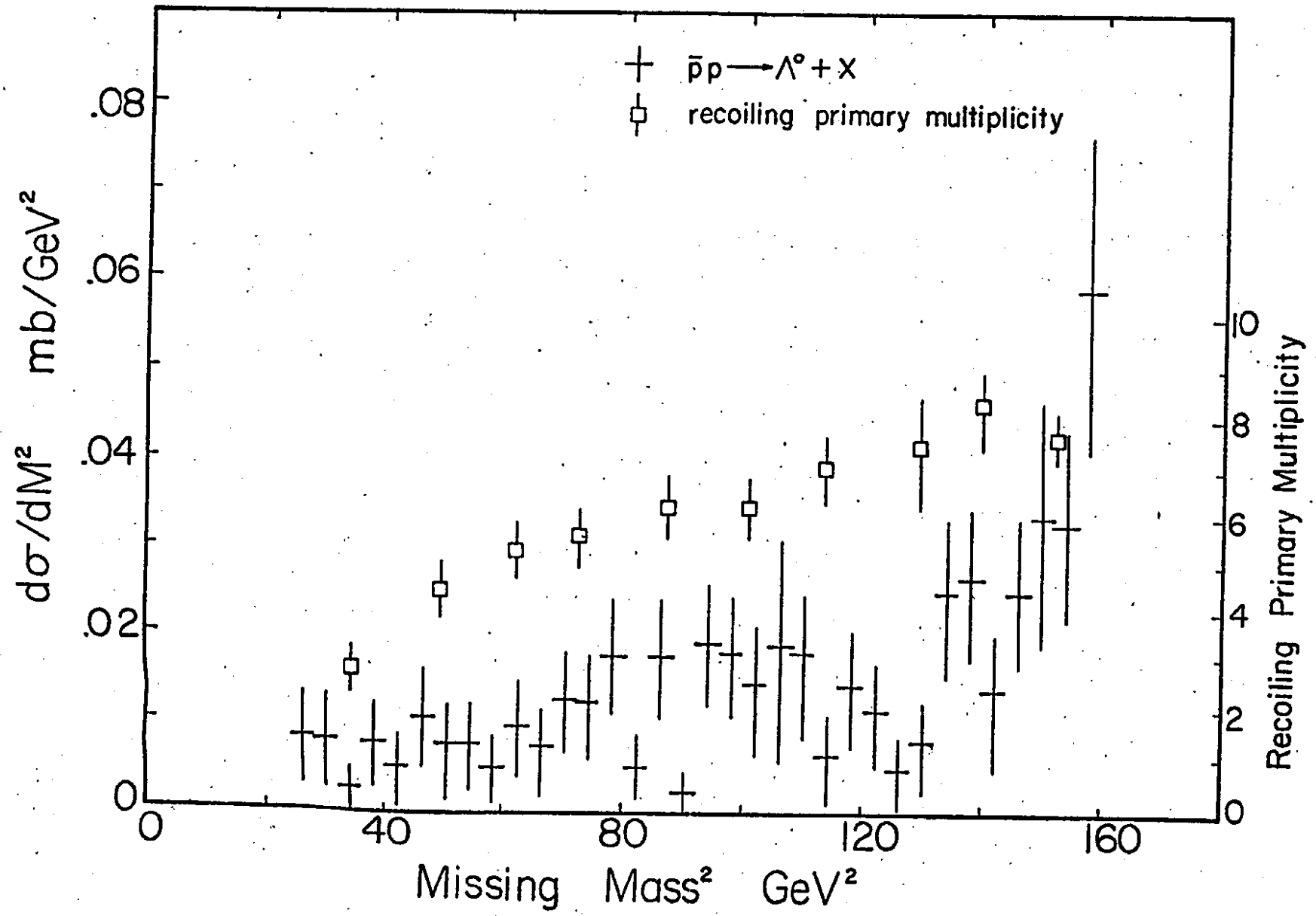
$\bar{p}p \longrightarrow \Lambda^0 + X$
recoiling primary multiplicity
$d\sigma/dM^2$ mb/GeV^2
.08
.06
.04
.02
0
0
40
80
120
160
Missing Mass^2 GeV^2
10
8
6
4
2
0
Recoiling Primary Multiplicity

Fig. 10 (c)

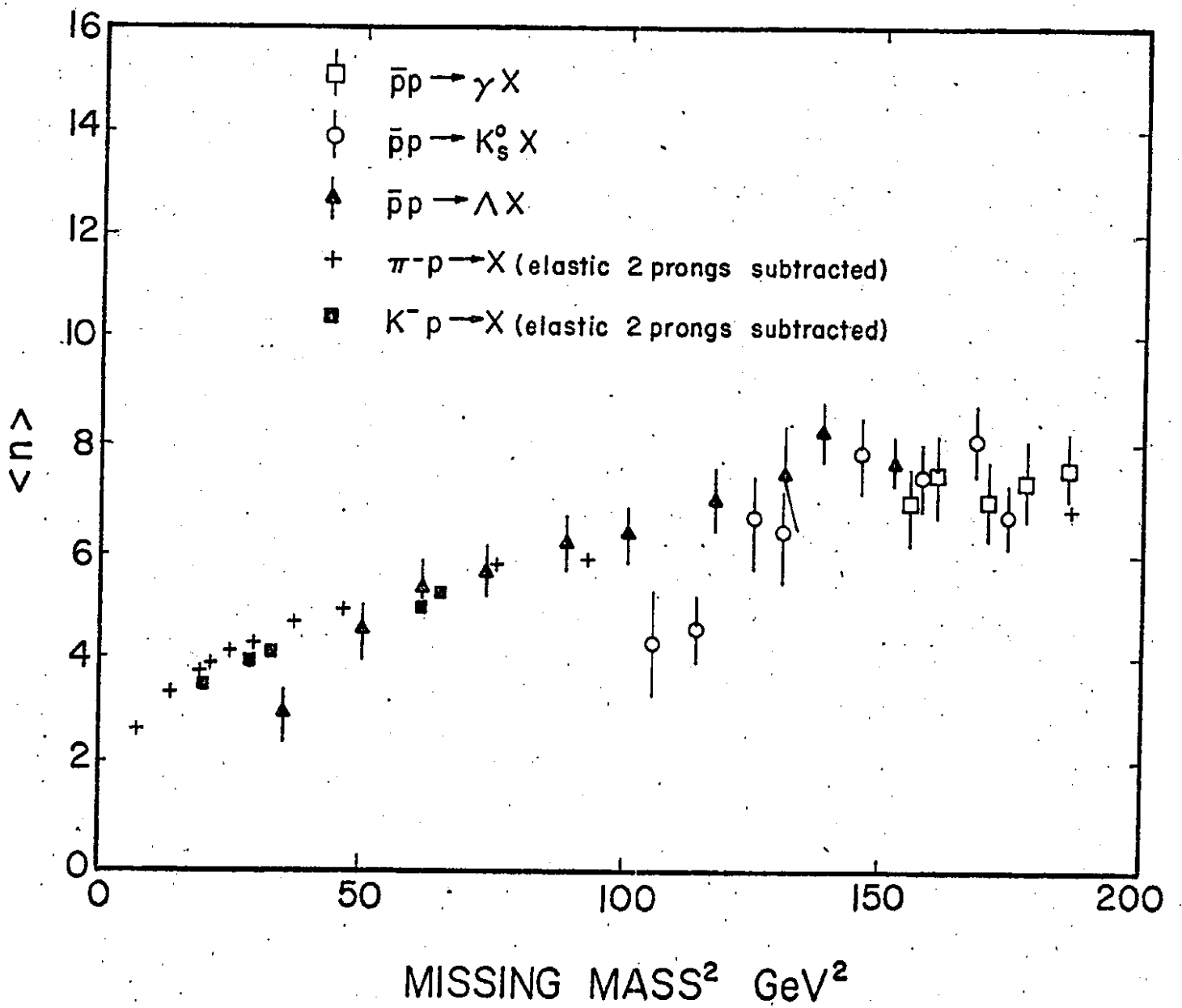
$\bar{p}p \to \gamma X$
$\bar{p}p \to K^0_s X$
$\bar{p}p \to \Lambda X$
$\pi^- p \to X$ (elastic 2 prongs subtracted)
$K^- p \to X$ (elastic 2 prongs subtracted)
$\langle n \rangle$
0
2
4
6
8
10
12
14
16
0
50
100
150
200
MISSING MASS^2 GeV^2

Fig. 11

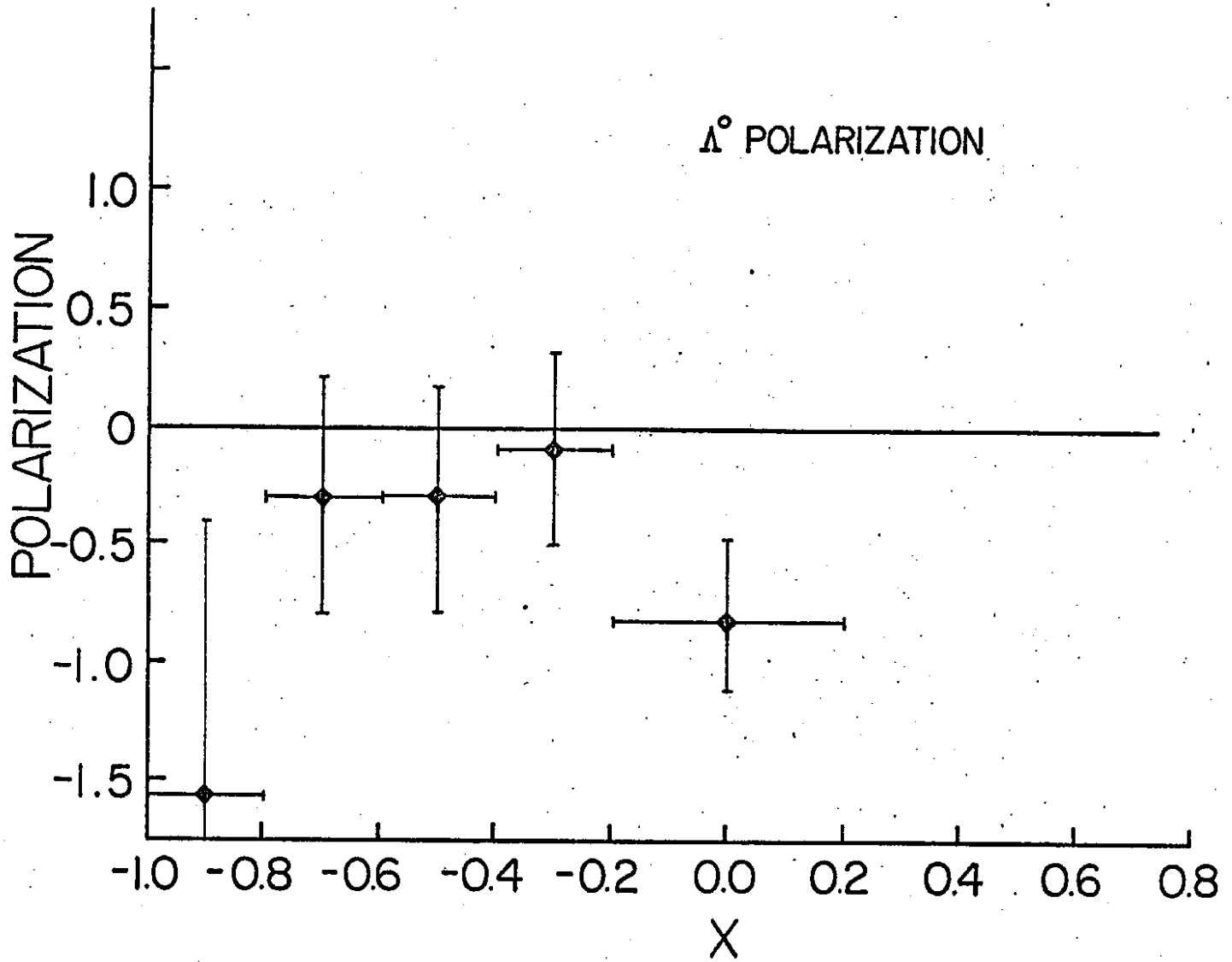
Λ° POLARIZATION
POLARIZATION
1.0
0.5
0
-0.5
-1.0
-1.5
-1.0
-0.8
-0.6
-0.4
-0.2
0.0
0.2
0.4
0.6
0.8
X

Fig. 12

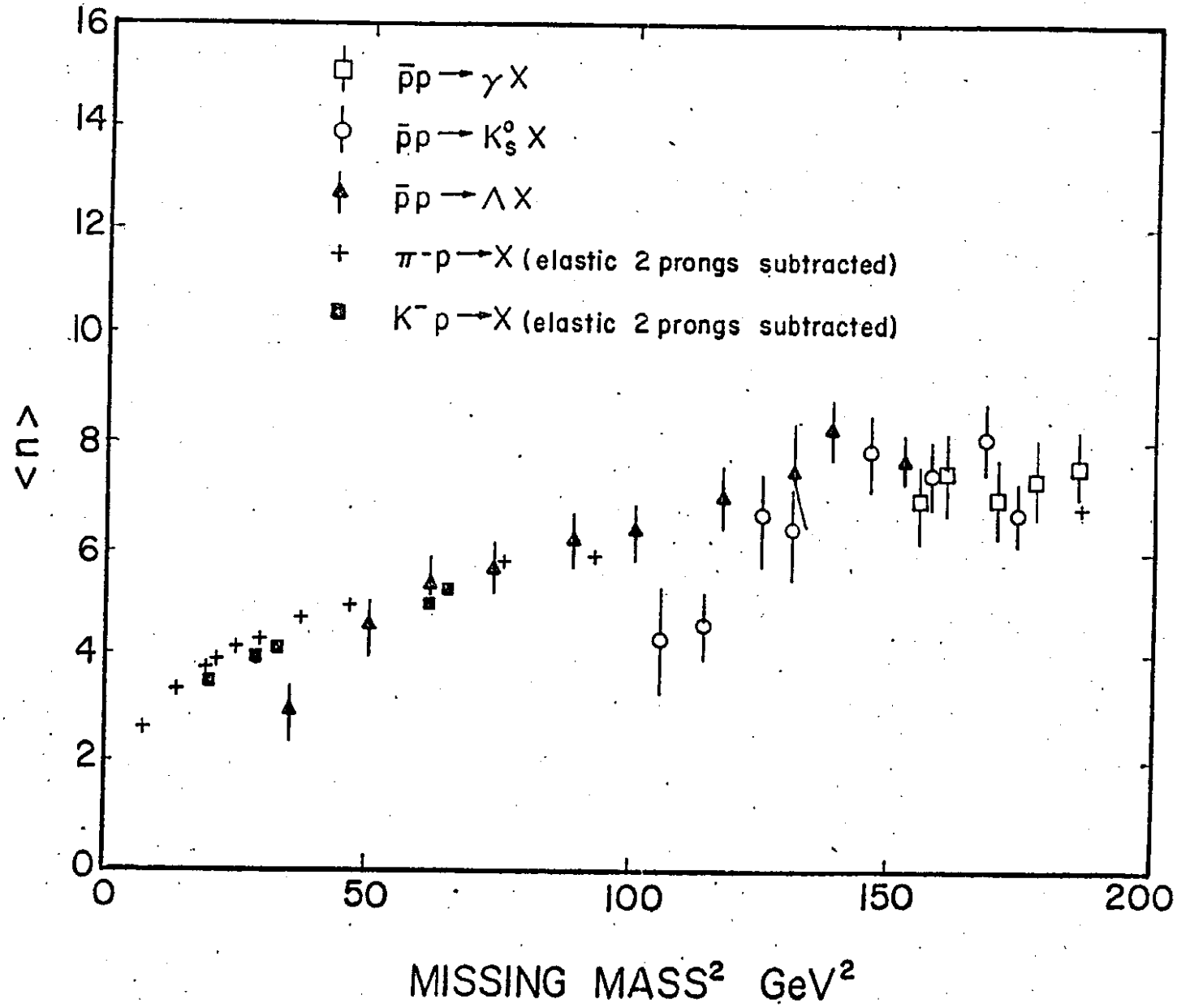
$\bar{p}p \to \gamma X$
$\bar{p}p \to K^0_s X$
$\bar{p}p \to \Lambda X$
$\pi^- p \to X$ (elastic 2 prongs subtracted)
$K^- p \to X$ (elastic 2 prongs subtracted)
$\langle n \rangle$
0
2
4
6
8
10
12
14
16
0
50
100
150
200
MISSING MASS^2 GeV^2

Fig. 11

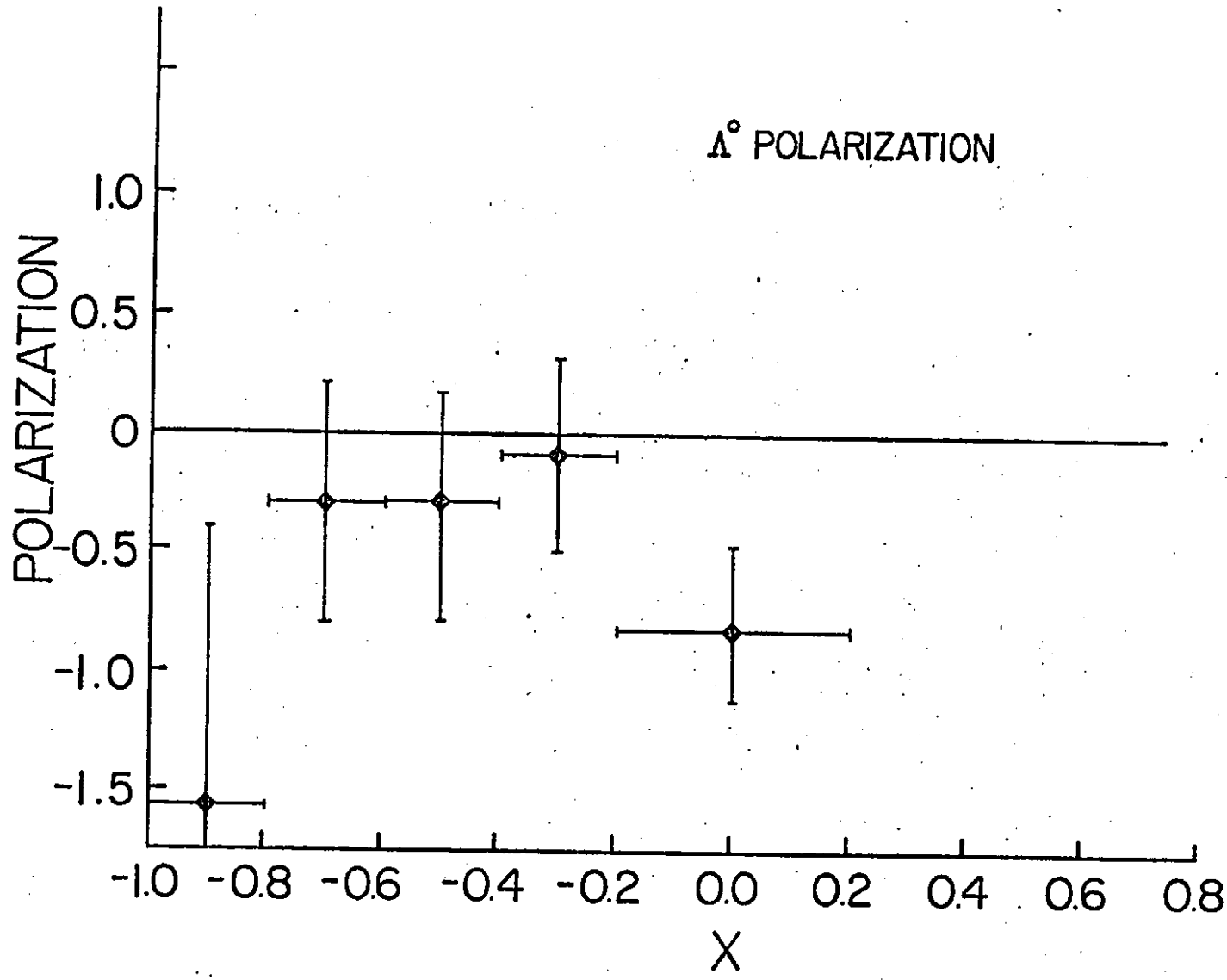
Λ° POLARIZATION
POLARIZATION
1.0
0.5
0
-0.5
-1.0
-1.5
-1.0
-0.8
-0.6
-0.4
-0.2
0.0
0.2
0.4
0.6
0.8
X

Fig. 12